Fundamentals of low-pressure nanofiltration: Membrane characterization, modeling, and understanding the multi-ionic interactions in water softening

Citation: Labban, Omar, Chang Liu, Tzyy Haur Chong, and John H. Lienhard V. "Fundamentals of Low-Pressure Nanofiltration: Membrane Characterization, Modeling, and Understanding the Multi-Ionic Interactions in Water Softening." Journal of Membrane Science 521 (January 2017): 18-32.

As Published: http://dx.doi.org/10.1016/j.memsci.2016.08.062

Publisher: Elsevier

Persistent URL: http://hdl.handle.net/1721.1/105440

Version: Author's final manuscript: final author's manuscript post peer review, without publisher's formatting or copy editing

Fundamentals of Low-Pressure Nanofiltration: Membrane Characterization, Modeling, and Understanding the Multi-Ionic Interactions in Water Softening

Omar Labban[a], Chang Liu[b,c], Tzyy Haur Chong[b,c], John H. Lienhard V[a,*]

[a] *Center for Clean Water and Clean Energy, Department of Mechanical Engineering, Massachusetts Institute of Technology, Cambridge MA 02139-4307, USA*

[b] *School of Civil and Environmental Engineering, Nanyang Technological University, Singapore 639798, Singapore*

[c] *Singapore Membrane Technology Centre, Nanyang Environment and Water Research Institute, Nanyang Technological University, Singapore 637141, Singapore*

Abstract

Recently, a novel class of low-pressure nanofiltration (NF) hollow fiber membranes, particularly suited for water softening and desalination pretreatment have been fabricated in-house using layer-by-layer (LbL) deposition with chemical crosslinking. These membranes can operate at exceedingly low pressures (2 bar), while maintaining relatively high rejections of multivalent ions. In spite of their great potential, our understanding as to what makes them superior has been limited, demanding further investigation before any large-scale implementation can be realized. In this study, the Donnan-Steric Pore Model with dielectric exclusion (DSPM-DE) is applied for the first time to these membranes to describe the membrane separation performance, and to explain the observed rejection trends, including negative rejection, and their underlying multi-ionic interactions. Experiments were conducted on a spectrum of feed chemistries, ranging from uncharged solutes to single salts, salt mixtures, and artificial seawater to characterize the membrane and accurately predict its performance. Modeling results were validated with experiments, and then used to elucidate the working principles that underlie the low-pressure softening process. An approach based on sensitivity analysis shows that the membrane pore dielectric constant, followed by the pore size, are primarily responsible for the selectively high rejections of the NF membranes to multivalent ions. Surprisingly, the softening process is found to be less sensitive to changes in membrane charge density. Our findings demonstrate that the unique ability of these membranes to exclusively separate multivalent ions from the solution, while allowing monovalent ions to permeate, is key to making this low-pressure softening process realizable.

Keywords: nanofiltration; low-pressure softening; layer-by-layer (LbL) deposition; characterization; solute transport and partitioning; negative rejection; seawater.

O. Labban, C. Liu, T.H. Chong, J.H. Lienhard V, "Fundamentals of Low-Pressure Nanofiltration: Membrane Characterization, Modeling, and Understanding the Multi-Ionic Interactions in Water Softening," J. Membrane Sci., online 31 August 2016, 521:18-32, 1 January 2017.

*Corresponding author: lienhard@mit.edu

Nomenclature

Roman Symbols

a_i	Solute activity, mol/m^3
A	Debye–Hückel constant, m$^{3/2}$/mol$^{1/2}$
A_k	Membrane porosity
c_i	Solute concentration, mol/m^3
d_i	Fiber inside diameter, m
d_o	Fiber outside diameter, m
$D_{i,p}$	Diffusion coefficient in the pore, m^2/s
$D_{i,\infty}$	Diffusion coefficient in the bulk, m^2/s
e	Elementary charge, 1.602×10^{-19} C
F	Farady constant, 96487 C/mol
I	Ionic strength, mol/m^3
J_i	Solute flux, mol/m^2· s
J_v	Permeate flux, m^3/m^2· s
k	Boltzmann constant, 1.38066×10^{-23} J/K
$k_{c,i}$	Solute mass transfer coefficient, m/s
$K_{i,c}$	Convection hindrance factor
$K_{i,d}$	Diffusion hindrance factor
L	Module length, m
N_A	Avogadro's number, 6.023×10^{23} mol^{-1}
Pe	Péclet number
r_p	Effective pore radius, m
r_i	Solute Stokes radius, m
R	Universal gas constant, 8.314 J/mol K
Re	Reynolds number
R_i	Rejection ratio
Sc	Schmidt number
Sh	Sherwood number
T	Temperature, K
x	Position across membrane active layer, m
X_d	Membrane charge density, mol/m^3
z_i	Ion valency

Greek Symbols

δ	Thickness of concentration polarization layer, m
ΔP	Applied pressure, Pa
ΔW_i	Born solvation energy barrier, J
Δx	Thickness of membrane active layer, m
ε_0	Permittivity of vacuum, 8.854×10^{-12} F/m
ε_b	Relative permittivity/dielectric constant of the bulk
ε_p	Relative permittivity/dielectric constant of the pore
ε_r	Relative permittivity/dielectric constant
γ_i	Activity coefficient
λ_i	Ratio of solute Stokes radius to effective pore radius
μ	Solution viscosity, Pa $\cdot$ s
μ_i	Solute electrochemical potential, J/mol
ϕ_i	Ratio of permeate flux to the uncorrected mass transfer coefficient
Φ_i	Steric partitioning coefficient
Φ_B	Born solvation coefficient
ψ	Electric potential, V
ξ	Electric potential gradient at the feed/membrane interface, V/m
Ξ_i	Mass transfer coefficient correction factor

Subscripts

b	Bulk solution in the feed
D	Donnan
i	Solute identity
lim	Limiting rejection
w	Membrane wall/feed interface just outside the pores
p	permeate

Superscripts

$\bullet$	Mass transfer correction for the suction effect

1. Introduction

Nanofiltration (NF) is a membrane separation process, first recognized in the late 1980's, whose performance is intermediate between that of reverse osmosis (RO) and ultrafiltration (UF), with a pore size on the order of one nanometer and a corresponding molecular weight cut-off (MWCO) of $300 - 500$ Da [1]. Generally, NF membranes are either positively or negatively charged depending on the feed chemistry and the functional groups forming the surface, and their separation performance is governed by the interplay of different mechanisms, namely steric effects (size exclusion), electrostatic effects (Donnan exclusion), as well as dielectric exclusion. The distinguishing characteristics of NF membranes — such as their ability to retain small organic molecules, higher selectivity towards monovalent ions, in addition to lower operating pressures and higher fluxes compared to RO membranes — promoted their adoption across a wide spectrum of applications, ranging from water and wastewater treatment [2, 3, 4] to food and textile engineering [5, 6, 7] as well as pharmaceutical and biotechnology applications [8, 9, 10]. A recent review by Mohammad et al. demonstrates the surging interest in the environmental applications of NF, which surpassed any other areas, from membrane fabrication to economics and design, based on the number of publications since 2008 [11].

Most commercial NF membranes are thin film composite (TFC) flat sheet membranes fabricated using interfacial polymerization, such as the NF series by Dow, the UTC series from Toray, and the Desal series by GE-Osmonics. Meanwhile, a variety of alternative methods to fabricate NF membranes have also been explored by researchers, including modified interfacial polymerization [12, 13], grafting polymerization [14], and nanomaterials embedment [15]. Recently, the successful development of a novel class of NF hollow fiber membranes has been demonstrated, fabricated using the layer-by-layer (LbL) polyelectrolyte deposition method with chemical crosslinking [16, 17]. Among all the membranes investigated in that study [17], it was proven that the LbL1.5C membrane was best suited for low-pressure softening applications. The results underscored the membrane's superior water softening capacity when compared to the state-of-the-art in softening, and to commercial NF membranes (NF 270 and NF 90) operating under low pressures (less than 5 bar), potentially opening doors for scale-up implementation of the membrane in low-pressure hard water softening and seawater desalination pretreatment.

In spite of these developments in NF low-pressure softening, however, further progress demands a deeper understanding of the fundamentals underlying the NF process. Unfortunately, NF separation of multi-ionic solutions is often difficult to predict given the complex nature of the interactions that occur among the ions themselves, and the ions and the membrane [18]. A rigorous model becomes essential to understand what governs the separation process and what transport and membrane properties dictate the softening performance, before we can extend our NF softening capabilities even further.

Earlier studies on NF modeling, geared at softening applications, exemplify the challenges encountered in this area, and demonstrate the need for further investigation. In their work on bipolar softening membranes, Soltanieh and Mousavi [19] implemented a modified version of the two-dimensional capillary model. Their work, however, was specifically targeted at bipolar membranes and only investigated the solute rejection as

a function of pH and polyelectrolyte concentration [19].

Bodzek et al. followed by looking into the application of both, the DS-5-DK NF membrane and the DS-3-SE RO membrane developed by Osmonics, to softening of well and tap water. Their results showed that NF, while being more permeable than RO, has sufficient selectivity and is more suited for softening applications [20]. In search of a deeper insight, however, Wesolowska et al. later extended this analysis by attempting to apply the DSPM-DE model to the DS-5-DK NF membrane only to conclude that the model cannot successfully be calibrated to real multi-ionic water solutions [21]. Results from these studies among others [18, 22], in addition to the recent developments in low-pressure softening membranes [12, 16, 17], underscore the pressing need for a comprehensive NF model applied to softening studies, featuring multi-ionic solutions at salinities approaching those of seawater.

Given the complexity associated with modeling transport and separation at a scale only one order of magnitude above atomic dimensions, NF modeling has been an active area of research for more than two decades. Since Tsuru et al. first proposed a model based on the extended Nerst-Planck equation to describe NF [23], the majority of modeling accounts in literature have largely been based on this approach. Two such models, the space-charge pore (SCPM) model and the Teorell-Meyer-Sievers (TMS) model, were investigated for potential NF modeling by Wang and coworkers. The SCPM assumes a porous membrane with radial distribution of potential and concentration, and requires an efficient means of solving the Poisson-Boltzmann equation along with the extended Nerst-Planck equation. The TMS model, on the other hand, assumes a homogeneous membrane with a uniform distribution of potential and concentration [24].

Subsequently, Bowen and Mukhtar proposed a hybrid model (HM) that assumes a nonporous membrane, yet introduces hinderance factors to account for the hindered transport [25]. Later atomic force microscopy (AFM) results introduced by Bowen et al. proved the existence of discrete pores in NF membranes, suggesting that a porous model is more consistent. Based on the results they obtained by assuming a uniform distribution in the pores, nonetheless, Bowen et al. concluded that the additional complexity borne by the SCPM model is not justified, and the term "Donnan-Steric Pore Model" (DSPM) was first coined [26]. In spite of DSPM's great success with simple solutions such as that of uncharged solutes, dyes, and univalent electrolytes [27], its accuracy was challenged when applied to mixtures of electrolytes and multivalent ions [28]. Consequently, dielectric exclusion was later incorporated as a partitioning mechanism by Bowen et al. [29]. This paved the way for the development of the Donnan-Steric Pore Model with dielectric exclusion (DSPM-DE) by Bandini and Vezzani [30], the open source program, NanoFiltran, by Geraldes and Alves [31], and lately the large-scale models for NF flat-sheet and spiral-wound modules by Roy et al. [32].

Despite the substantial efforts on modeling single salt solutions and ternary ionic mixtures, a subject fairly established and well understood in NF literature, very few studies specifically targeting multi-ionic mixtures, such as artificial seawater, currently exist. This shortcoming is exacerbated by the scarcity of results available on modeling softening, which are necessary for understanding and optimizing the process. Although significant progress has been made on the fabrication-front when it comes to the novel NF hollow

fiber membranes introduced earlier [12, 16, 17], a lot remains to be done as no formal attempt has been made to model these membranes. The transport and partitioning mechanisms underlying their performance, in addition to what properties makes this new class of membranes particularly promising for softening, remain obscure. To the best of our knowledge, no specific efforts in literature have been made to investigate which of the membrane properties in the DSPM-DE model dominate a separation process, and what implications that could have on our understanding of low-pressure NF softening.

In this study, the DSPM-DE model is adopted for the first time to predict the softening performance of a cross-linked LbL NF membrane, similar to the LbL1.5C membrane presented by Liu et al. [17] . The objective is to provide and validate a rigorous approach to characterizing the membrane, offer a complete description of the softening process involved, and extend our current understanding of low-pressure NF softening. Experiments on uncharged solutes, ternary ionic mixtures, and multi-ionic solutions, including artificial seawater, were carried out, and the resulting trends, including negative rejection, were investigated. The nature of the multi-ionic interactions among the ions themselves, and the ions and the membranes are elucidated for the different hard water feeds considered in the study. An approach based on sensitivity analysis is proposed to determine the membrane property that dominates the softening process. Our results show that the membrane effective pore size and pore dielectric constant (and surprisingly not the membrane charge density) are the two parameters that dominate the softening process for this membrane.

2. Theoretical Background

To model the separation performance of nanofiltration membranes, transport inside the membrane as well as in the concentration polarization layers has to be considered as shown in Fig. 1. While a typical TFC membrane is composed of an active layer and a porous support layer, the membrane separation is dictated solely by its membrane active layer [33], and hence, the support layer can reasonably be ignored throughout our analysis. In addition to the membrane active layer, the occurrence of concentration polarization on the feed/membrane and membrane/permeate interfaces, which can also undermine the membrane performance, must be considered.

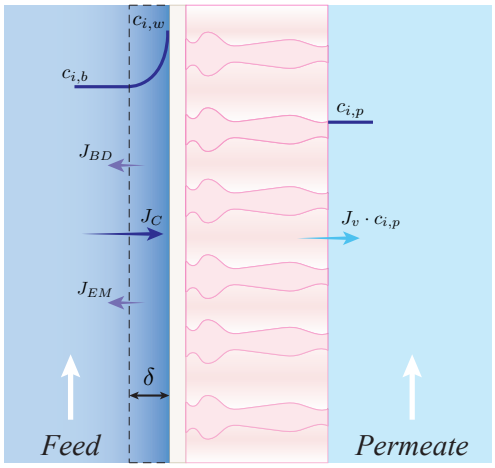

Figure 1: Schematic illustration of solute transport across a NF membrane. A feed solution is separated from the permeate solution by virtue of the membrane interface. Due to the nature of selective solute transport across the membrane, concentration polarization (CP) occurs at the surface. The net solute flux can be expressed as the sum of the convective, diffusive, and electromigrative contributions across the CP layer.

In light of these requirements, we start our modeling approach by an account of the main equations that govern solute transport inside the membrane active layer. We then move on to concentration polarization outside the active layer, and lay out an approach to account for its effects. Afterwards, our system of equations is closed with the incorporation of solute partitioning under electrochemical equilibrium. Finally, a brief overview of the discretization process necessary to numerically solve the system is provided.

2.1. Modeling Transport in the Membrane Active Layer

In the membrane active layer, the flux of the i^{th} solute, J_i, may be expressed in terms of the gradient in solute electrochemical potential as [29]:

$$J_i = -\frac{c_i D_{i,p}}{RT}\frac{d\mu_i}{dx} + K_{i,c} c_i J_v \tag{1}$$

$$D_{i,p} = K_{i,d} D_{i,\infty} \tag{2}$$

In Eq. 1, the solute electrochemical potential, assuming constant pressure and velocity in the pores, can be expressed as:

$$\mu_i = RT \ln a_i + z_i F \psi + \text{constant} \tag{3}$$

where a_i refers to the solute activity, respectively. By differentiating Eq. 3, and substituting the result back into Eq. 1, the extended Nerst-Planck equation is obtained [25]:

$$J_i = -D_{i,p}\frac{dc_i}{dx} + K_{i,c} c_i J_v - \frac{z_i c_i D_{i,p} F}{RT}\frac{d\psi}{dx} \tag{4}$$

The extended Nerst-Planck equation accounts for the transport of solutes through the membrane by diffusion, convection, and electromigration. The negative sign preceding the diffusive and electromigrative terms reminds us that transport through these mechanisms occurs down a gradient in concentration or electrical potential. Transport through convection, on the other hand, occurs as a result of the porous nature of NF membranes [26].

Given the scale of the pores in NF membranes, the mobility of the solutes through them is greatly reduced. The apparent rates of diffusion and convection are considerably lower in confining pores, relative to the bulk solution, when the pore and solute radii approach the same order. Under these circumstances, the transport is said to be "restricted" or "hindered" [34]. Hindered transport is accounted for in Eqs. 1 and 4 through the inclusion of $K_{i,d}$ and $K_{i,c}$, which are hindrance factors for diffusion and convection, respectively. These factors are expressed in terms of the ratio of the solute Stokes radius to the pore radius, λ_i, and are related to the solute enhanced drag and lag drag coefficients as explained elsewhere [35]. For solutes with $\lambda_i \leq 0.95$, $K_{i,d}$ may be expressed according to the result obtained by Dechadilok and Deen [35]:

$$K_{i,d} = \frac{\begin{array}{c} 1.0 + (9/8)\lambda_i \ln(\lambda_i) - 1.56034\lambda_i + 0.528155\lambda_i^2 + 1.91521\lambda_i^3 \\ - 2.81903\lambda_i^4 + 0.270788\lambda_i^5 - 1.10115\lambda_i^6 - 0.435933\lambda_i^7 \end{array}}{(1-\lambda_i)^2} \tag{5}$$

For solutes with $\lambda_i > 0.95$, $K_{i,d}$ was calculated using the result obtained by Mavrovouniotis and Brenner [36]:

$$K_{i,d} = 0.984\left(\frac{1-\lambda_i}{\lambda_i}\right)^{5/2} \tag{6}$$

Similarly, $K_{i,c}$ was calculated using Eq. 7 according to this result by Ennis et al. [37]:

$$K_{i,c} = \frac{1 + 3.867\lambda_i - 1.907\lambda_i^2 - 0.834\lambda_i^3}{1 + 1.867\lambda_i - 0.741\lambda_i^2} \tag{7}$$

Although the hollow fiber membranes modeled in this study are cylindrical in geometry and not flat, Cartesian coordinates can still be invoked in the analysis with reasonable accuracy under the condition that $\Delta x_e / d_o \ll 1$ [38], where Δx_e is the effective thickness of the membrane active layer and d_o is the fiber outside diameter. Apart from the extended Nerst-Planck equation, electroneutrality accounting for the membrane charge density X_d also needs to be satisfied:

$$X_d + \sum_{i=1}^{N} z_i c_i = 0 \tag{8}$$

2.2. Concentration Polarization and Mass Transfer Modeling

Concentration polarization refers to the formation of concentration gradients on the membrane feed and permeate interfaces as different constituents of the feed solution permeate through the membrane at different rates. This change in concentrations at the membrane interfaces leads to a reduction in permeate flux and rejection ratios. Concentration polarization can occur at the feed/membrane interface given the membrane

selectivity at the active layer, and at the membrane/permeate interface as the membrane contacts a permeate enriched in one of the feed solution components. This effect can be controlled by adjusting the velocities in the feed and permeate channels, among other techniques [39]. For most membrane processes with bulk fluid flow through the membrane, concentration polarization on the permeate side, which is usually dilutive in salt-rejecting membranes, may reasonably be neglected [33].

Concentration polarization on the feed/membrane interface was accounted for using the model developed by Geraldes and Afonso [40]. According to their model, the net flux of solute i is expressed as the sum of the fluxes due to back diffusion, convection, and electromigration, as illustrated in Fig. 1.

$$J_i = -k_{c,i}^{\bullet}(c_{i,w} - c_{i,b}) + J_v c_{i,w} - z_i c_{i,w} D_{i,\infty} \frac{F}{RT} \xi \tag{9}$$

where ξ refers to the electric potential gradient at the feed/membrane interface, $c_{i,w}$ is the solute concentration at the feed/membrane interface just outside the pores, and $c_{i,b}$ is the bulk concentration, respectively. Under steady state operating conditions, the flux continuity equation for solute i may also be expressed in terms of the permeate concentration $c_{i,p}$:

$$J_i = J_v c_{i,p} \tag{10}$$

Note that the diffusive flux in Eq. 9 is expressed in terms of a mass transfer coefficient, $k_{c,i}^{\bullet}$, determined from conventional Sherwood number correlations, and corrected for the "suction effect" caused by membrane permeation at the interface through the inclusion of the flux-dependent correction factor, Ξ, as follows [40]:

$$k_{c,i}^{\bullet} = k_{c,i} \Xi \tag{11}$$

$$\Xi = \phi_i + (1 + 0.26\phi^{1.4})^{-1.7} \tag{12}$$

with $\phi_i = J_v / k_{c,i}$. The mass transfer coefficient, $k_{i,c}$, was evaluated using the Sherwood number correlation for laminar flow in a tube with fully developed velocity profile, and developing concentration profile [41]:

$$\mathrm{Sh}_i = 1.62 \mathrm{Re}^{0.33} \mathrm{Sc}_i^{0.33} (d_i / L)^{0.33} \tag{13}$$

with Re being the flow Reynolds number, Sc_i the solute Schmidt number, d_i the fiber inside diameter, and L the length of the module.

In addition to the concentration polarization equations developed in this section, two electroneutrality conditions should also be met in the feed and permeate regions. The first of these conditions, Eq. 14, applies at the feed/membrane interface, while the second condition, Eq. 15, applies in the permeate region [31]. These conditions take the form:

$$\sum_{i=1}^{N} z_i c_{i,w} = 0 \tag{14}$$

$$\sum_{i=1}^{N} z_i c_{i,p} = 0 \tag{15}$$

2.3. Solute Partitioning at Electrochemical Equilibrium

While diffusive fluxes act to eliminate concentration gradients in bulk solutions, concentration gradients can still exist in "true equilibrium" across a selective medium under certain conditions, such as a charged membrane [42]. The difference in concentration between a membrane's pores and the bulk solution is commonly referred to as solute partitioning, and plays a significant role in a membrane's selectivity towards solutes. Two additional expressions are obtained from describing solute partitioning under electrochemical equilibrium at the feed/membrane and membrane/permeate interfaces. These expressions are obtained by setting the electrochemical potential equal on both sides of an interface. In this derivation, we will refer to the solution inside the pores with a prime and consider a general interface for convenience:

$$\mu_i = \mu_i' \tag{16}$$

Substituting our definition for the electrochemical potential from Eq. 3, and accounting for solute nonidealities through the introduction of an activity coefficient yields:

$$\frac{\gamma_i c_i}{(\gamma_i c_i)'} = \exp\left(- \frac{z_i F}{RT} \psi_D \right) \tag{17}$$

In Eq. 17, which resembles the Nerst equation, ψ_D refers to the Donnan potential forming across the membrane at equilibrium [43, 42, 44]. The activity coefficient is calculated using Davies model, which relates γ_i to the solution ionic strength, I, through the semi-empirical relation [45, 46]:

$$\ln(\gamma_i) = -A z_i^2 \left(\frac{\sqrt{I}}{1+\sqrt{I}} - bI \right) \tag{18}$$

$$I = \frac{1}{2} \sum_{i=1}^{N} z_i^2 c_i \tag{19}$$

where b is assigned a value of 0.3 herein. A is the temperature-dependent Debye–Hückel constant expressed as [46, 47]:

$$A = \left(\frac{\sqrt{2\pi N_A}}{\ln(10)} \right) \left(\frac{e^2}{4\pi\varepsilon_0\varepsilon_r kT} \right)^{3/2} \tag{20}$$

with N_A being Avogadro's number, e the elementary charge, ε_0 the permittivity of vacuum, ε_r the solvent's dielectric constant or relative permittivity, and k the Boltzmann constant.

Apart from the Donnan exclusion/partitioning mechanism expressed in Eq. 17 and in agreement with Donnan theory, other solute partitioning mechanisms occur across a NF membrane for which Eq. 17 fails to account. Based on geometric [34] as well as thermodynamic arguments [48], Eq. 17 has been modified in literature through the introduction of a steric term, which accounts for sieving effects that arise as a result of the finite size of the solute relative to the pore, quantified by the parameter λ_i [27].

$$\frac{\gamma_i c_i}{(\gamma_i c_i)'} = \Phi_i \exp\left(- \frac{z_i F}{RT} \psi_D \right) \tag{21}$$

$$\Phi_i = (1 - \lambda_i)^2 \tag{22}$$

In addition to sieving and Donnan effects, evidence from electrochemical studies in colloidal systems suggests that the solvent's dielectric constant is considerably reduced in the membrane's confining pores relative to the bulk solution [29]. This difference in dielectric constant between the bulk solution and the membrane pores presents a barrier to ion solvation into the pores, as predicted by Born model, which leads to a higher ion rejection ratio. This partitioning mechanism is referred to as dielectric exclusion, is indifferent to the ionic charge, and becomes more significant with increasing ion valency. The dielectric exclusion mechanism has been extensively investigated in literature [30, 49], and is incorporated into Eq. 21 by the introduction of a Born solvation coefficient, Φ_B, with ΔW_i being the solvation energy barrier computed in accordance with Born model [44]:

$$\frac{\gamma_i c_i}{(\gamma_i c_i)'} = \Phi_i \Phi_B \exp\left(- \frac{z_i F}{RT} \psi_D \right) \tag{23}$$

$$\Phi_B = \exp\left(- \frac{\Delta W_i}{kT} \right) \tag{24}$$

$$\Delta W_i = \frac{z_i^2 e^2}{8\pi\varepsilon_0 r_i} \left(\frac{1}{\varepsilon_p} - \frac{1}{\varepsilon_b} \right) \tag{25}$$

where r_i is the solute Stokes radius, ε_p is the dielectric constant of the pore, and ε_b is the dielectric constant of the bulk solution.

Applying Eq. 23 to account for solute partitioning at the feed/membrane and membrane/permeate interfaces, the two additional expressions necessary are obtained. These expressions act as "boundary conditions" on the membrane interfaces with the feed and permeate solutions, and become increasingly important when solving for the concentration profile across the membrane. In writing these expressions, we follow the notation presented by Geraldes and Alves [31], where Eq. 26 describes the partitioning as it occurs just inside and just outside the membrane at the feed/membrane interface, and Eq. 27 describes partitioning as it occurs just inside and just outside the membrane at the membrane/permeate interface (Fig. 2):

$$\frac{\gamma_{i,1} c_{i,1}}{(\gamma_{i,w} c_{i,w})} = \Phi_i \Phi_B \exp\left(- \frac{z_i F}{RT} \psi_{D,w} \right) \tag{26}$$

$$\frac{\gamma_{i,N} c_{i,N}}{(\gamma_{i,p} c_{i,p})} = \Phi_i \Phi_B \exp\left(- \frac{z_i F}{RT} \psi_{D,p} \right) \tag{27}$$

Implicit in this derivation has been the assumption of electrochemical equilibrium, which might appear to be in contradiction with the observation that a finite flux of ions is always being transported across the membrane. The equilibrium assumption derives its validity from a primary restriction inherent in membrane transport models. This restriction is related to the equilibrium assumption and the way it is applied only across the feed/membrane interface or the membrane/permeate interface, and not the entire membrane as one entity. Stated differently, the equilibrium assumption contends that the fluids on both sides of the membrane are in equilibrium with the membrane itself. This assumption implies that the gradient in chemical potential

across the membrane will have to be continuous at all points inside and outside the membrane for equilibrium to exist, which certainly is a reasonable assumption under steady-state operating conditions [33].

2.4. Membrane Discretization and Modeling

The expressions derived thus far represent the equations that govern the transport and partitioning of solutes across a NF membrane at steady-state operating conditions. A complete account of these phenomena is obtained when the membrane active layer is discretized into nodes, as illustrated in Fig. 2, and one extended Nerst-Planck equation is applied for every solute at every node. These equations are coupled with the concentration polarization equation and the boundary conditions derived from solute partitioning to form a closed system that is solved numerically. Our numerical approach is in tandem with that presented by Geraldes and Alves [31].

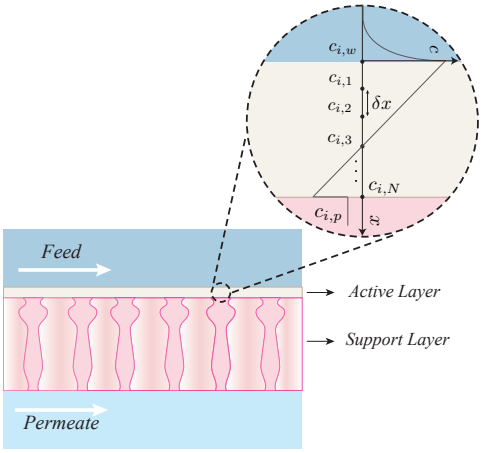

Figure 2: Modeling transport across a NF membrane. The membrane active layer is discretized into N nodes, separated by a spacing of δx, and one NP equation is applied for each solute at every node. These equations are coupled with the partitioning/boundary conditions to form a closed system. In this illustration, $c_{i,w}$ refers to the concentration at the membrane wall just outside the pores, while $c_{i,1}$ refers to the concentration just inside the wall. A similar relationship exists between $c_{i,p}$ and $c_{i,N}$.

3. Materials and Methods

3.1. Materials

The polyethersulfone (PES) ultrafiltration hollow fiber substrate was produced in-house similar to our previous studies [50, 51]. The inner and outer diameters of the substrate are 1.0 and 1.4 mm, respectively, with the pure water permeability of around 350 LMH/bar and the molecular weight cut-off (MWCO) of 50 kDa. Poly(allylamine hydrochloride) (PAH, Sigma Aldrich, Mw $= 120 - 200$ kDa), and poly(styrenesulfonic acid) sodium salt (PSS, Alfa Aesar, Mw $= 500$ kDa) were used to make polyelectrolyte solutions with sodium chloride (NaCl, Merck) as the supporting electrolyte. Glutaraldehyde solution (GA, 50% in water) was obtained from Sigma Aldrich as the crosslinking agent. Sodium chloride (NaCl), calcium chloride ($CaCl_2$),

sodium sulfate (Na_2SO_4), magnesium sulfate ($MgSO_4$) and magnesium chloride ($MgCl_2$) (Merck) were used for charged solute tests. The pH of solutions was adjusted using hydrochloric acid (HCl, fuming, 37%) and sodium hydroxide (NaOH) obtained from Merck. Neutral organic solutes such as glycerol, glucose and sucrose were purchased from Merck and used for uncharged solute rejection tests. DI water was produced by a Milli-Q system (Millipore, USA).

3.2. Layer-by-layer deposition and crosslinking

The detailed procedures of the semi-dynamic inner surface modification were reported in our previous studies [16, 17] and briefly described below. Fifteen pieces of dried hollow fibers were sealed into PTFE membrane modules with an effective length of 25 cm. The LBL deposition and GA crosslinking at the lumen surface were performed by introducing the polyelectrolyte and the GA solution throughout the fiber lumen with a syringe and maintained for a desired contact time, followed by DI water rinse after each step. Membrane modules were then stored in DI water for characterization and performance evaluation. The morphology of the NF membrane was examined by a Field Emission Scanning Electron Microscope (FE-SEM JSM-7600F, JEOL, Japan), and is depicted in Fig. 3.

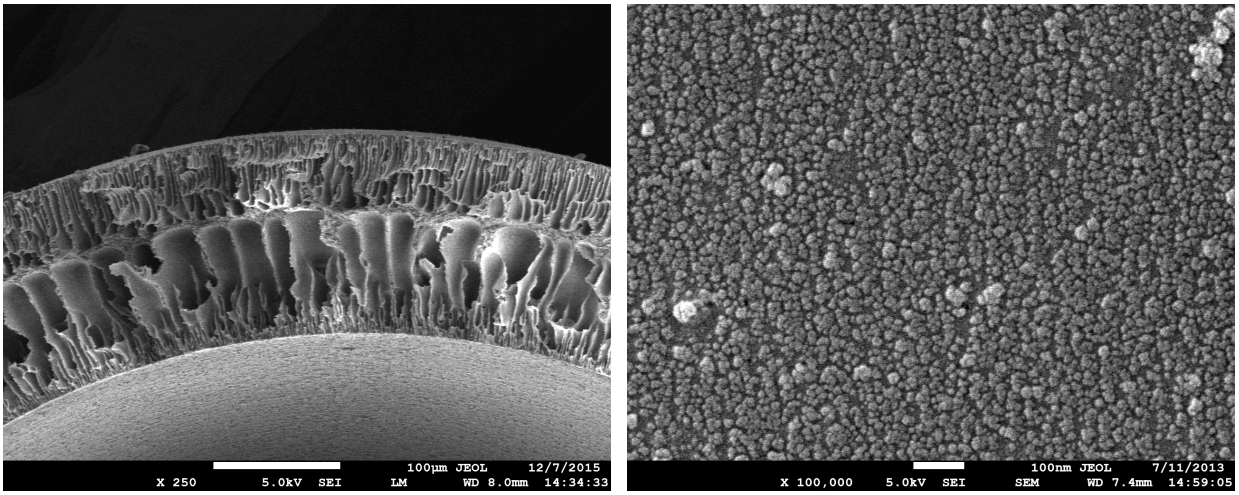

Figure 3: The morphology of the LbL-C membrane as examined by a Field Emission Scanning Electron Microscope. (a) Membrane cross section ×250. (b) Membrane inner surface ×100000.

3.3. NF performance tests

The pure water permeability of the NF membrane was measured on a bench scale cross-flow filtration unit, as shown in Fig. 4, under a varied transmembrane pressure (TMP) from 1 to 4 bar using DI water. Inside-out filtration was performed for the hollow fibers.

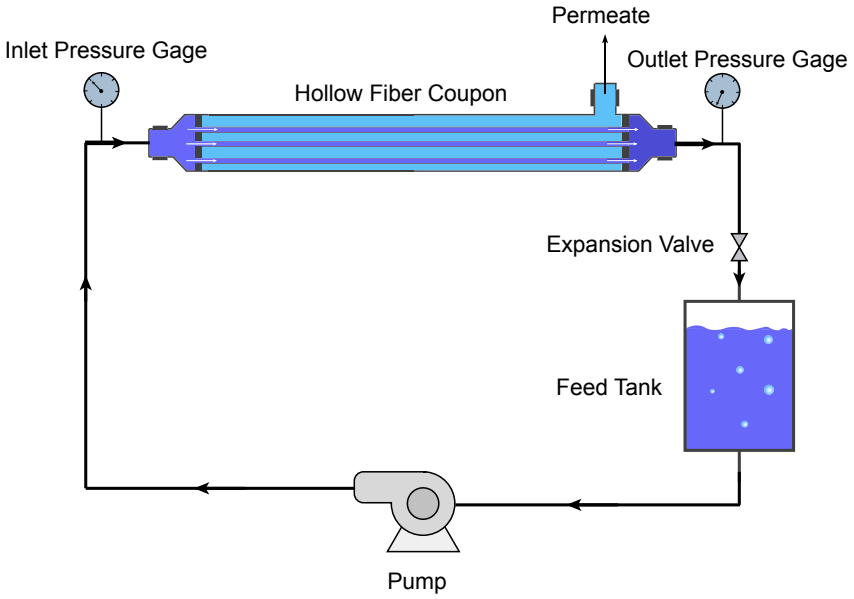

Figure 4: Cross-flow filtration unit used in running NF performance tests. Feed water is pumped through a bench-scale hollow fiber system, and later expanded back via an expansion valve for recirculation. Filtration experiments were conducted using uncharged solutes (200 mg/kg), single salts (1000 mg/kg NaCl / pH range: $5-9$), and salt mixtures (NaCl+$MgCl_2$, NaCl+$NaSO_4$, artificial seawater). Transmembrane pressure (TMP) varied from 1 to 4 bar, and a cross-flow velocity of 0.3 m/s was maintained. Results obtained from three membrane modules were averaged before testing results were reported.

The uncharged salt rejection tests of the NF membrane were performed on the same unit using 200 mg/kg solutions of glucose, sucrose and glycerol, while varying TMP from 1 to 4 bar. A relatively high cross-flow velocity (0.3 m/s) was maintained for the salt solution flow to minimize the concentration polarization effect. The rejection of the neutral organic solutes was obtained from the concentrations of the feed and permeate solutions based on the total organic carbon measurements using a TOC analyzer (TOC-VCSH, Shimadzu, Japan).

The charged solute rejection tests, including single salt and mixed salt solutions, of the NF hollow fiber membrane were determined by the same unit under varied TMP from 1 to 4 bar and a fixed cross flow velocity of 0.3 m/s. The single salt rejection tests were conducted using 1,000 mg/kg NaCl with solution pH ranging from 5 to 9, based on the conductivity measurements (Ultrameter II, Myron L Company, Canada) of the permeate and feed water. For the mixed salt solution tests, cation and sulfate concentrations in the feed and permeate solutions were determined by an inductively coupled plasma optical emission spectrometry (ICP-OES, Optima 8000, Perkin Elmer, USA). All of the rejection tests were repeated for three membrane modules and the averaged results were reported.

4. Results and Discussion

4.1. Membrane Characterization

One crucial aspect of membrane modeling involves characterizing the membrane in terms of parameters that allow it to be described with reasonable accuracy using simplified mathematical models. The process of membrane characterization in NF literature has undergone considerable changes over time as the models grew in sophistication. In the early nonporous hybrid model (HM) introduced by Bowen and Mukhtar, NF membranes were only characterized by two parameters, the effective membrane charge and thickness [25]. With the introduction of the porous DSPM model, the membrane effective pore size was then added and coupled with the effective membrane thickness through the Hagen-Poiseuille equation [26]. Realizing the importance of the process as a prerequisite to running any model, Bowen and Mohammad later developed a simplified characterization method, and applied it to 29 NF membranes from 10 manufacturers [52]. The membrane pore dielectric constant was eventually added to the list of membrane parameters to account for dielectric exclusion [29].

The membrane characterization approach adopted in this study was inspired by the earlier work of Bowen and Mohammad [27] and Bowen and Welfoot [29]. In our approach, a set of 4 experiments are necessary to accurately characterize the membrane. The effective membrane pore size and thickness are first determined from uncharged solute and pure water permeability experiments. These are followed by the membrane pore dielectric constant and effective membrane charge, which are determined from single salt experiments at different pH values, and mixed salt experiments. The solute properties used in this process and later in the study are summarized in Tables 1 and 2 for reference.

Table 1: Uncharged Solute Properties.

Solute	Molecular Weight (g/mol)	r_i (nm)	D_∞ ($m^2/s \times 10^{-9}$)
Atrazine	215	0.390	0.553
Glycerol	92	0.260	0.950
Glucose	180	0.365	0.690
Sucrose	342	0.471	0.520
Xylose	150	0.300	0.769

Table 2: Charged Solute Properties.

Ion	Molecular Weight (g/mol)	r_i (nm)	D_∞ ($m^2/s \times 10^{-9}$)
Na^+	23	0.184	1.33
Ca^{+2}	40	0.309	0.792
Mg^{+2}	24	0.347	0.706
Cl^-	35	0.121	2.03
SO_4^{2-}	96	0.230	1.06

4.1.1. Defining an Effective Pore Size: Uncharged Solute Experiments

The first step in the membrane characterization process involves the estimation of an effective pore size. The approach presented in this section follows the one presented first by Bowen et al. [26], and relies on running rejection experiments on uncharged solutes. In their work, Bowen et al. derive a closed form expression for the real rejection of uncharged solutes that is only a function of the membrane effective pore size and thickness. The result they obtained took the form:

$$R_{real} = 1 - \frac{c_{i,p}}{c_{i,w}} = 1 - \frac{K_{i,c}\Phi_i}{1 - \exp(-\mathrm{Pe}_w)[1 - \Phi_i K_{i,c}]} \tag{28}$$

$$\mathrm{Pe}_w = \frac{K_{i,c}}{K_{i,d}} \frac{J_v \Delta x_e}{D_{i,\infty}} \tag{29}$$

where Pe_w is the Péclet number that compares the convective relative to diffusive transport through the pores, and $K_{i,d}$, $K_{i,c}$, and Φ_i are calculated according to Eqs. 6, 7, and 22, respectively. This expression takes into account concentration polarization by considering the feed concentration at the membrane interface $c_{i,w}$ to calculate the real rejection, rather than the observed rejection. By allowing the Péclet number to take on increasingly larger values and convection to dominate membrane transport, a new expression for rejection is obtained, called "limiting rejection" [26]:

$$R_{\mathrm{lim}} = 1 - K_{i,c}\Phi_i \tag{30}$$

Empirical evidence shows that uncharged solute rejection increases with increasing permeate flux as convection becomes more dominant, and the permeate becomes less concentrated. What Eq. 30 underscores is the fact that beyond a certain value for rejection, denoted by R_{lim}, increasing the flux does not contribute to increasing rejections. Beyond this point, any increase in convective transport is offset by the increasing concentration polarization and solute transport across the membrane. This phenomenon of limiting rejection will later be encountered in our study, and has been reported elsewhere as well [26, 29, 53].

For Eqs. 28 - 30 to be helpful in membrane characterization, experimental results obtained for "real rejections" are required before values for an effective pore size and thickness can be fitted. To minimize the impact of concentration polarization on the fluxes obtained in experiments, uncharged solute experiments

were run on glycerol, glucose, and sucrose at low concentrations (200 mg/kg) and relatively high crossflow velocities (Re $\sim$ 400). Under this setup and the low pressures of interest, the resulting real and observed rejections would be very close. The results obtained from running uncharged solute experiments, while operating between 1 and 4 bar, are summarized in Table 3. With these results, an average pore radius of 0.5 nm was estimated, along with the values of the effective membrane thickness fitted for each solute according to Eqs. 28 and 29. These results are provided in Table 4.

Table 3: Uncharged Solute Experimental Results.

Pressure Applied	1 bar	2 bar	3 bar	4 bar
Glycerol Rejection (%)	11	15	19.5	29
Glucose Rejection (%)	74	77	83	83
Sucrose Rejection (%)	93	94	93	92

Table 4: Membrane Modeling Parameters.

Solute	λ_i	r_p (nm)	Δx_e (μm)
Glycerol	0.520	0.5	1.6
Glucose	0.730	0.5	1.2
Sucrose	0.942	0.5	1.0

Since uncharged solute rejection is indifferent to dielectric exclusion and Donnan effects, the DSPM-DE model was run using the values reported in Table 4, assuming $X_d = 0$ and $\varepsilon_p = \varepsilon_b = 80.4$, under exceedingly larger values of permeate flux and crossflow velocity to estimate the "limiting rejection" of each solute. These results are plotted in Fig. 5 against the limiting rejection curve, which is defined by Eq. 30. The good agreement observed between the values obtained for limiting rejection using an effective pore radius of 0.5 nm and the limiting rejection curve suggest that this pore size can be used as the effective membrane pore size for all subsequent analysis [27]. It should be noted, however, that successfully defining a membrane effective pore size does not guarantee the existence of such well-defined cylindrical pores in the membrane, nor does it imply the presence of a uniform pore size distribution throughout it. Instead, defining an effective pore size only implies that the hindered transport of solutes across a given membrane is equivalent to their transport across pores of this effective size [25].

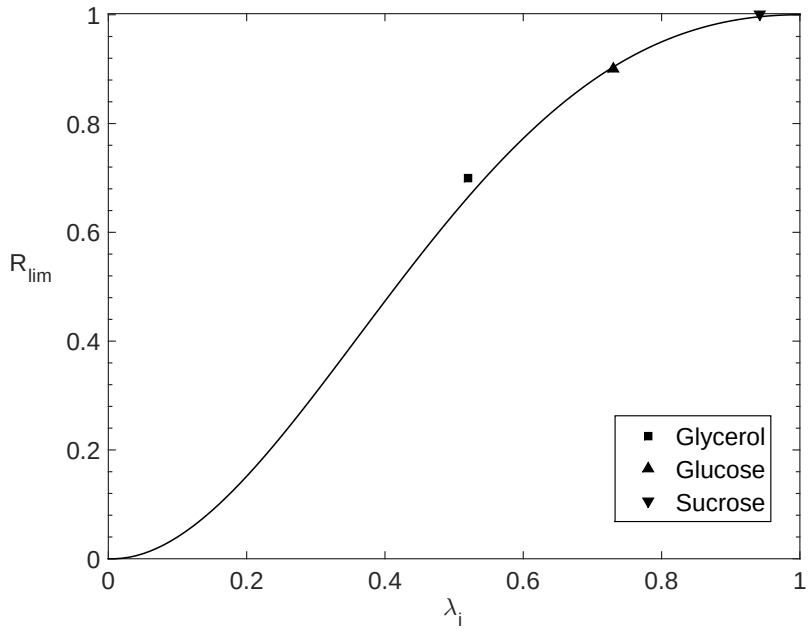

Figure 5: Plot of limiting rejection as a function of λ_i. The values of solute limiting rejections for the LbL-C membrane were estimated using the DSPM-DE model, and are plotted. The good agreement between the limiting rejection curve and these limiting rejections establish 0.5 nm as an effective pore radius for the LbL-C membrane.

4.1.2. Defining an Effective Membrane Thickness: Pure Water Permeability Experiments

The membrane effective thickness, defined as the ratio of the membrane thickness Δx to its porosity A_k, can be estimated based on the Hagen-Poiseuille equation once an effective pore size is established [26, 52]. Assuming the pores are cylindrical and uniform in size, the permeate volumetric flux is given by:

$$J_v = \frac{r_p^2 \Delta P}{8\mu \Delta x_e} \tag{31}$$

with ΔP being the applied pressure, and μ the solution viscosity. Pure water permeability experiments, summarized in Fig. 6, provide evidence in support of a linear relationship between permeate flux and applied pressure. Given the value of r_p defined in Section 4.1.1 along with Eq. 31 and the experimental results in Fig. 6, the effective membrane thickness, Δx_e, was estimated to be 1.33 μm, agreeing closely with the results reported earlier in Table 4. Similar to r_p, this value of Δx_e will be assumed constant for all subsequent analysis in this study.

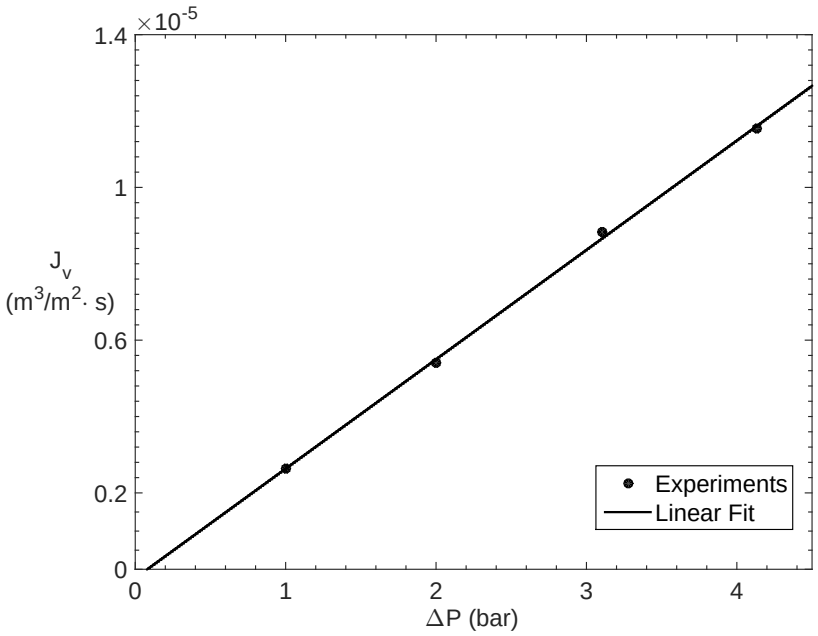

Figure 6: Pure water permeability (PWP) experiments for the LbL-C membrane. Under these operating conditions, the applied pressure and permeate flux were linearly correlated. The membrane's average PWP was found to be around 10 LMH/bar.

4.1.3. Defining a Pore Dielectric Constant: Single Salt pH Experiments

Once the effective membrane pore size and thickness have been determined, the next step in membrane characterization involves estimating the membrane pore dielectric constant, ε_p. Fig. 7 illustrates the results obtained for the rejection of a 1000 mg/kg NaCl solution as a function of pH. As shown in the figure, the salt rejection initially decreases with increasing pH and reaches a minimum, before it starts increasing again. The point at which rejection is minimum is commonly referred to as the membrane "isoelectric point" (IEP), and is considered to be the point at which the membrane is uncharged [29]. Accordingly, this limits the membrane's partitioning mechanisms to steric partitioning and dielectric exclusion only, allowing for the pore dielectric constant to be determined by least squares fitting.

According to Fig. 7, the membrane IEP occurs between a pH of 7.0 and 8.0. To evaluate ε_p, least squares fitting was used to match the experimental results at a pH of 7.0 and 8.0, assuming the membrane is uncharged. The values obtained for ε_p from the analysis varied by less than 6% over this range. In this study, the IEP was taken at a pH of 7.0, which falls in line with the results of the zeta-potential analysis carried out by Liu et al. [17], with a corresponding $\varepsilon_p = 41.3$, which will also stay constant for all subsequent analysis. To summarize, the DSPM-DE modeling parameters fitted for the LbL-C membrane from experimental results are listed in Table 5. This leaves only one degree of freedom, the membrane charge density, X_d, which will be our next subject of discussion.

Table 5: LbL-C DSPM-DE Parameters

Parameter	r_p (nm)	Δx_e (μm)	ε_p
	0.5	1.33	41.3

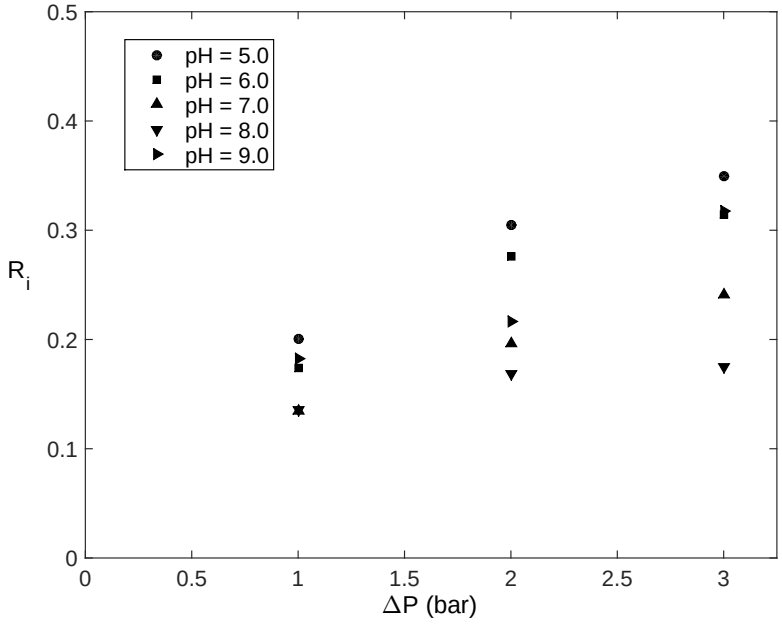

Figure 7: Rejection as a function of applied pressure and pH for single salt experiments (1000 mg/kg NaCl). The isoelectric point (IEP) for the LbL-C membrane occurs between a pH of 7.0 and 8.0.

4.1.4. Hard Water and Artificial Seawater Experiments

Estimating the membrane charge density, X_d, is the final stage of the membrane characterization process. Unfortunately, however, the membrane charge density is not only a function of the membrane, but is also sensitive to variation in feed composition and pH. Depending on the feed pH and composition, ion adsorption to the membrane [26] as well as dissociation of the membrane functional groups [54] could occur, ultimately affecting the membrane charge. In some instances, counterion adsorption has been reported, leading to complete shielding or even inversion of the membrane charge [55]. For these reasons, estimates of the membrane charge density are feed-specific at best. This leaves one degree of freedom when modeling any NF membrane using the DSPM-DE model. One way of handling this limitation has been the adoption of Freundlich isotherms, which express the membrane charge as a function of concentration based on empirical data [25, 27].

To study the softening performance of the LbL-C membrane and investigate its selectivity to various feeds, experiments were run on hard water of varying chemistries. The feeds examined, whose compositions are summarized in Table 6, include an NaCl+$MgCl_2$ and an NaCl+Na_2SO_4 salt mixtures, in addition to an

artificial seawater solution. The experimental results obtained for individual ion rejection and permeate flux as a function of applied pressure are listed in Tables 7 - 9. The estimated membrane charge density using least squares regression was $X_d = 2.83$ mol/m^3 for the NaCl+$MgCl_2$ mixture, $X_d = -1.92$ mol/m^3 for the NaCl+$NaSO_4$ mixture, and $X_d = -27$ mol/m^3 for the artificial seawater mixture, respectively.

Table 6: Synthetic Hard Water Feed Compositions.

Ion Concentration (mg/kg)					
Salt Mixture	Na^+	Ca^{+2}	Mg^{+2}	SO_4^{2-}	Cl^-
NaCl + $MgCl_2$	398.6	–	254.2	–	1351
NaCl + Na_2SO_4	718.7	–	–	678.2	606
Artificial Seawater	11122	382	1394	2136	20300

Table 7: NaCl + $MgCl_2$ Observed Rejection.

NaCl + $MgCl_2$ Ion Rejection (%)				
Applied Pressure	Na^+	Mg^{+2}	Cl^-	Flux (LMH)
2 bar	−7.6	99.1	51.0	12.0
3 bar	−1.7	99.2	49.0	19.2
4 bar	1.6	99.0	51.0	26.4

Table 8: NaCl + Na_2SO_4 Observed Rejection.

NaCl + Na_2SO_4 Ion Rejection (%)				
Applied Pressure	Na^+	SO_4^{2-}	Cl^-	Flux (LMH)
2 bar	37.8	94.5	−9.0	14.2
3 bar	39.4	94.5	−7.0	23.1
4 bar	39.4	93.8	−6.0	31.6

Table 9: Seawater Experimental Rejection.

Artificial Seawater Ion Rejection (%)						
Applied Pressure	Na^{+}	Ca^{+2}	Mg^{+2}	SO_4^{2-}	Cl^{-}	Flux (LMH)
2 bar	−1.4	54.5	83.4	82.7	11	1.4
3 bar	−0.6	71.1	90.6	85.4	13	3.9
4 bar	1.17	78.9	93.6	86.8	15	6.0

4.2. Model Validation and Results

Characterization of the LbL-C membrane in the previous section sets the stage for validation of the DSPM-DE model and its applicability to this new class of low-pressure softening membranes. In this section, the DSPM-DE model is validated against the experimental results reported in Section 4.1 for uncharged and charged solutes. The observed trends, the underlying multi-ionic interactions, as well as insights obtained from the application of the model to the membrane are discussed.

4.2.1. Modeling Uncharged Solutes

To validate the model against uncharged solute experiments, modeling simulations were run while varying the transmembrane pressure. The modeling results, illustrated in Fig. 8, had an average deviation of 12% from the experimental results, demonstrating excellent agreement between modeling and experimental results. As explained earlier, our modeling results in Fig. 8 capture how solute rejection increases with increasing flux, as convection dominates, until a limiting value for rejection is reached. Since the effective membrane pore radius estimated (0.5 nm) was comparable to the Stokes radius of sucrose (0.471 nm), the model slightly overestimates its rejection. The results obtained also suggest that the LbL-C membrane has lower rejection for glycerol compared to glucose, falling inline with the observation that glycerol has a smaller Stokes radius and a relatively larger diffusivity according to Table 1.

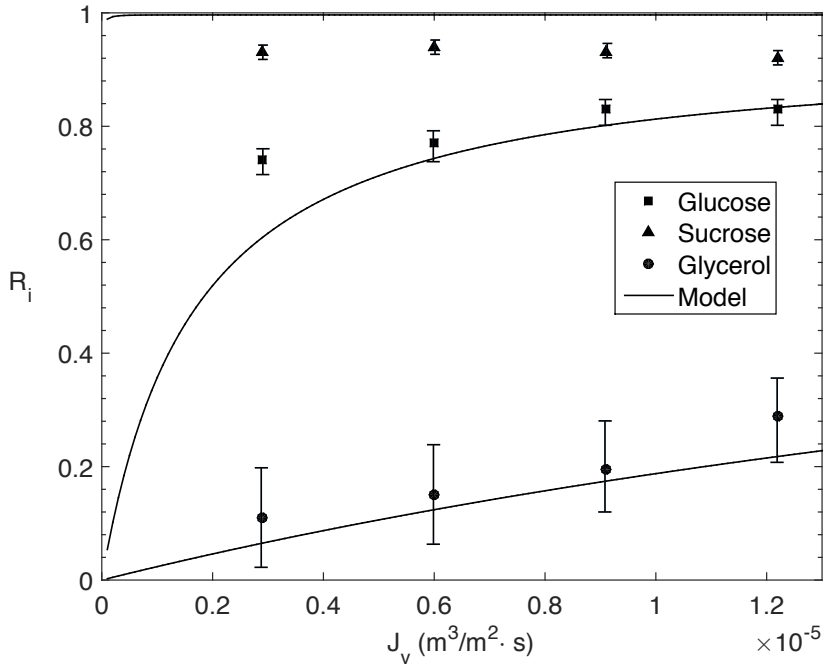

Figure 8: Experimental and modeled uncharged solute rejection as a function of permeate flux. Experiments were run using 200 mg/kg solutions of glycerol, glucose, and sucrose. Solute retention increased with increasing solute size or MW, and decreasing diffusivity. The average deviation between modeling and experimental results was 12%, validating the model's applicability to uncharged solutes. The error bars are based on 10% error in measuring the permeate concentration.

Following its validation, the model was run to predict the membrane's rejection to other solutes, namely atrazine and xylose, allowing us to investigate its performance over a wide spectrum of solutes. Similar to the results presented in Fig. 8, the obtained results reported in Fig. 9, demonstrate that the membrane's rejection towards uncharged solutes increases with increasing solute Stokes radius, or equivalently, decreasing solute diffusivity.

According to Table 1, the results in Fig. 9 suggest that solute rejection also increases with increasing molecular weight. Figure 10 underscores this fact by plotting rejection as a function of molecular weight. According to the figure, uncharged solute rejection increases steadily with increasing molecular weight, and jumps once the solute Stokes radius approaches the effective membrane pore size ($\lambda_i \to 1$), before it slowly plateaus at 1. Using a plot similar to Fig. 10 along with a properly calibrated model allows for the molecular weight cut-off (MWCO) to be estimated without additional experimentation. For instance, the MWCO of the LbL-C membrane can be estimated to be approximately 250 Da, which is close to the MWCO of 205 Da reported experimentally by Liu et al. [17]. Since rejections are a function of permeate flux, an even closer estimate of MWCO = 215 Da can be obtained from Fig. 9.

Since solutes are not perfect spheres, nor are membrane pores perfect cylinders, a plot similar to that in Fig. 10, while being qualitatively useful, should always be taken with scrutiny. Relying primarily on

molecular weight to predict rejection could be misleading, for instance, should the solute deviate considerably from spherical geometry. Since solute rejection for uncharged solutes is primarily size-based, higher values of uncharged solute rejection would be achievable primarily with a tighter membrane, whose effective pore size is smaller.

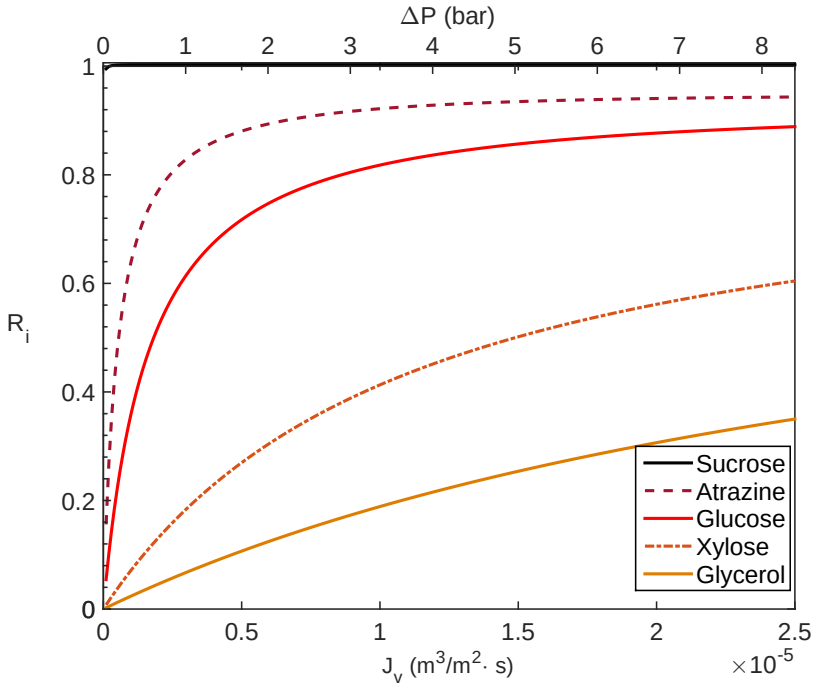

Figure 9: Predicting the LbL-C membrane performance for a variety of uncharged solutes as a function of applied pressure or permeate flux. Solute retention increased with increasing solute size or molecular weight, and decreasing solute diffusivity, indicating uncharged solute rejection is primarily a result of sieving effects. Solutes with greater retentions approached their limiting rejections faster. The system setup and flow conditions matched that of the experiments across all simulations.

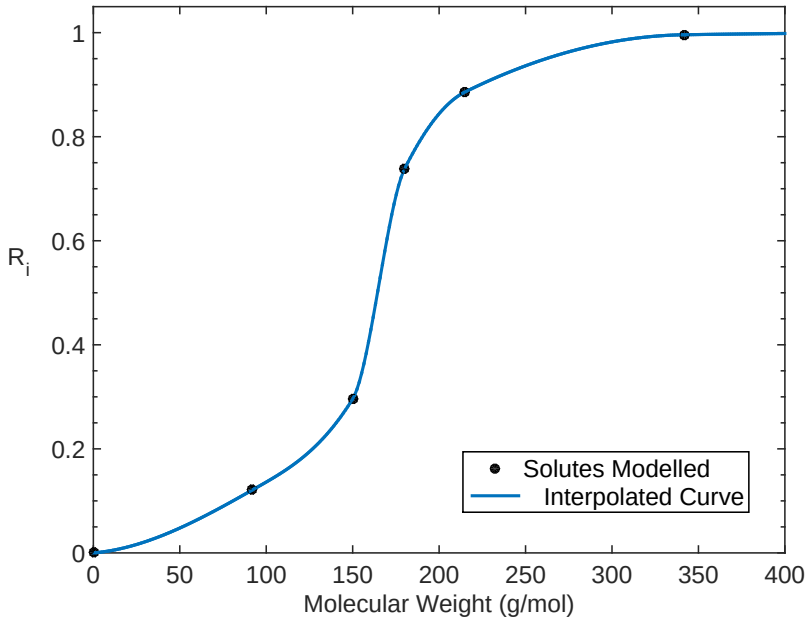

Figure 10: Plot of uncharged solute rejection as a function of solute molecular weight. Solute rejection increases with increasing molecular weight, and the molecular weight cut-off (MWCO) of the LbL-C can be estimated to be approximately 250 Da. Solute rejection increases dramatically as the MWCO is approached. The values reported in this figure correspond to an applied pressure of 2 bar.

4.2.2. Modeling Hard Water Mixtures: The Phenomenon of Negative Rejection

Figure 11 shows the results obtained from modeling the NaCl+$MgCl_2$ hard water mixture, which strongly agrees with experimental results. With the introduction of charged species into the feed chemistry, the selectivity of the NF membrane is now a function of not only steric hindrance (size-based), but also Donnan partitioning and dielectric electric exclusion, adding to the overall complexity of the system. Similar to other results obtained for uncharged solutes, rejection increases with increasing flux for this mixture. The membrane has superior retention to the multivalent ion, Mg^{+2}, which is around 99% even at applied pressures as low as 2 bar. This selectively high rejection towards multivalent ions is a characteristic of NF membranes, and primarily governed by dielectric exclusion as our study proves later. Given that this is a ternary ion system, the interesting phenomenon of "negative rejection" is observed and is well-predicted by the model. This phenomenon has been encountered extensively in literature [25, 56, 57], primarily as a result of the interaction between the different pairs of coions in the solution and the membrane, as will become evident.

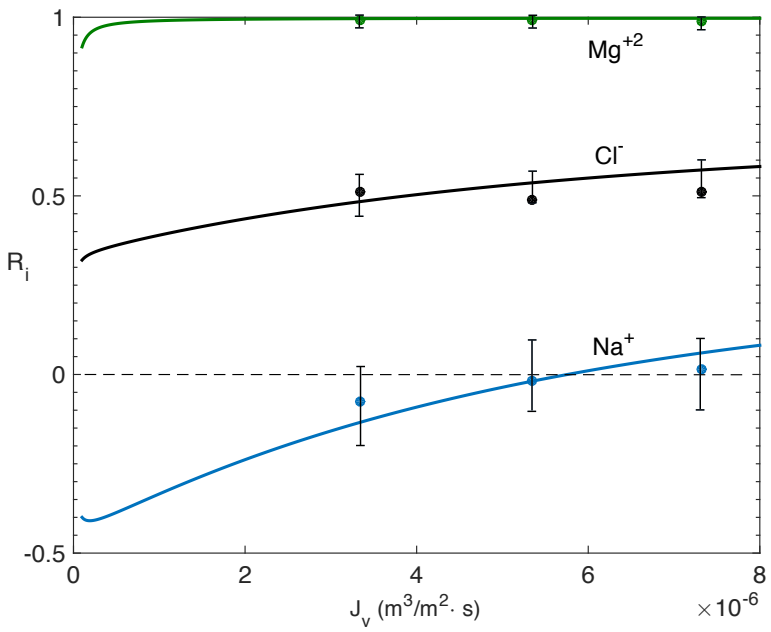

Figure 11: Experimental and modeling results for the rejection of the different ions in Mixture 1 as a function of permeate flux. The agreement between experiments and simulation results validates the model for this mixture, and the high rejection towards the multivalent ion at pressures as low as 2 bar demonstrates the softening capacity of the LbL-C membrane. The experimental values reported correspond to applied pressures of 2-4 bar. The error bars are based on 10% error in measuring the permeate concentration.

Fundamentally, negative rejection does not mean that mass (solute is this case) is being created, nor does it imply that the mixture now has more salts or ions than it initially started with. Negative rejection only implies that the system has a higher concentration of a given ion in the permeate, relative to the feed. In other words, negative rejection for a given ion species only occurs when more of that ion is in the smaller permeate volume relative to the much larger feed volume. The total number of ions is conserved, and only their relative allocation among the feed and permeate changes, primarily as a function of the membrane and ions in the solution.

Yaroshchuk provides a detailed account of negative rejection and the mechanisms that underlie its occurrence [58]. These include equilibrium mechanisms, kinetic mechanisms, and a possible combination of the two. Based on our simulation results, which clearly indicate that the concentration of the negatively rejected ion unintuitively decreases in the membrane relative to the bulk, kinetic mechanisms must be responsible. Taking an example of a ternary system with two cations and one anion (similar to Mixture 1), Yaroshchuk argues that negative rejection in this case results from the fundamental requirements of charge electroneutrality and zero electric current traversing the membrane. When dielectric exclusion starts playing a more prominent role in solute partitioning, Yaroshchuk contends that a "relative pull-in" of the less charged coion could even result [58].

In light of this account, a physical interpretation for negative rejection in our case is reached by looking

at the relevant transport mechanisms across the membrane in more detail. In the NaCl+$MgCl_2$ mixture, negative rejection of Na^+ cannot be a result of pure convective transport of the ions across the membrane. If we assume the membrane is completely passive towards to Na^+ (membrane does not see Na^+ to begin with), a lower bound of zero rejection will be observed. Zero rejection suggests that the membrane is passive (or indifferent) towards the Na^+ ions, and does not enhance nor restrict their transport, respectively. Since this is a lower bound, rejection cannot be lower; and hence, convective transport alone cannot be accountable, and does not explain the phenomenon. A similar analysis focused only on the diffusion of Na^+ leads to the same conclusion. Since diffusion acts to eradicate any concentration gradients across an interface, this transport mechanism cannot be responsible for reversing the concentration gradient, effectively making the permeate more concentrated than the feed. If neither convection nor diffusion of Na^+ can justify the negative rejection observed in experiments and predicted by our model, some other mechanism must be responsible.

The key point is the importance of the interaction between the different ions in the solution. On the feed side, the two cations, Na^+ and Mg^{+2}, are neutralized by the only anion in the mixture, Cl^-. This is consistent with the fact that the concentration of Cl^- exceeds that of Na^+ in the feed, as Table 6 shows. Driven by a gradient in electrochemical potential and a low rejection by the membrane, the Cl^- ions are transported from the feed to the permeate. Since the membrane is impermeable to Mg^{+2} by virtue of its selectivity (dielectric exclusion), the more mobile Na^+ ions are the only counterions available to neutralize the permeate solution. In effect, the transported Cl^- ions will "pull in" the extra Na^+ ions with them so that charge electroneutrality is always satisfied on both sides of the membrane. Stated differently, the transport of Na^+ ions is enhanced by the counterion, Cl^-, which leads to a higher concentration of Na^+ ions in the permeate and results in the apparent negative rejection. The same phenomenon was observed with the other synthetic water feeds studied, and a similar explanation applies to the trends seen.

A similar behavior was observed with the NaCl+$NaSO_4$ mixture as can be seen from Fig. 12. The membrane has high retentions towards the multivalent ion, SO_4^{2-}, with rejection ratios close to 95% at applied pressures as low as 2 bar. This low operating pressure is possible given the high membrane selectivity towards the monovalent ions, which constitute the majority of the mixture. Similar to the NaCl+$MgCl_2$ mixture, the more mobile coion, Cl^- in this case, is negatively rejected by the membrane. Given that the membrane is impermeable to SO_4^{2-} and that Cl^- is the only anion available to neutralize the transported Na^+ ions on the permeate side, the observation of negative rejection for Cl^- falls directly inline with our previous explanation.

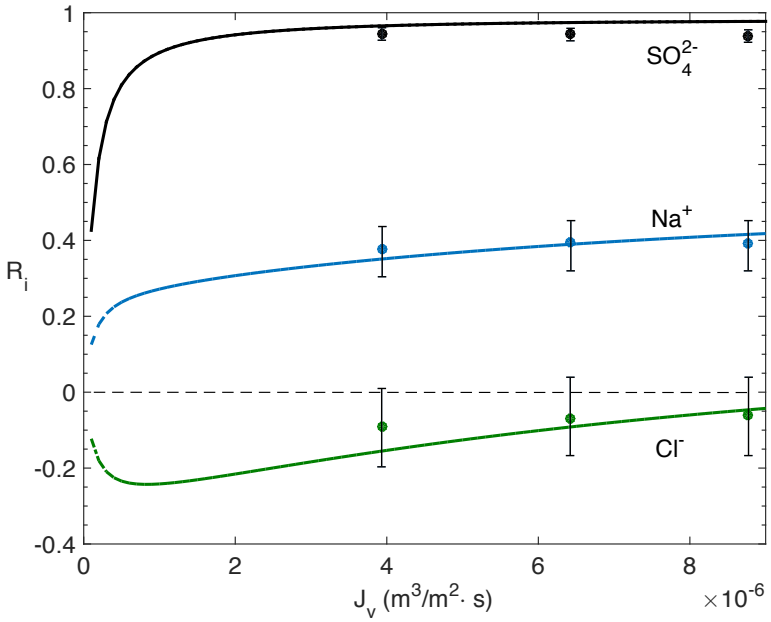

Figure 12: Experimental and modeling results for the rejection of the different ions in Mixture 2 as a function of permeate flux. The agreement between experiments and simulation results validates the model for this mixture, and the high rejection towards the multivalent ion at pressures as low as 2 bar demonstrates the softening capacity of the LbL-C membrane. The experimental values reported correspond to applied pressures of 2-4 bar. The error bars are based on 10% error in measuring the permeate concentration.

Rather than being indifferent to solute transport (zero rejection), a membrane with "negative rejection" essentially enhances the transport of that solute or ion across it. This ion is usually the more mobile coion in the mixture, and this phenomenon tends to be desirable when the target is to eliminate the less mobile ion (Mg^{+2} or SO_4^{2-}in this case). For softening applications specifically, rejection towards the multivalent ions is the primary factor of interest. Being able to "selectively pick" the multivalent ions only, while intentionally allowing the monovalent ions to permeate, allows for softening to be carried out more economically, and at much lower energy penalties, as was observed with the LbL-C membrane (less separation work is necessary). In addition, the negative rejection of monovalent ions allows the permeate of the LbL-C to have a higher osmotic pressure relative to the permeate of other NF membranes that partially reject monovalent as well multivalent ions. This higher osmotic pressure on the permeate side reduces the osmotic pressure difference across the membrane, leading to lower applied pressures than otherwise would be necessary to reach the same permeate flux. Together, these reasons elucidate the mechanics underlying low-pressure softening, and why this membrane fared well when compared to other commercial membranes in the experimental study by Liu et al. [17].

4.2.3. Modeling Artificial Seawater

Figure 13 shows the results obtained based on our model and experiments for artificial seawater. The high concentrations, the nature of the ionic interactions that occur among the ions themselves, along with

the interactions between the ions and the membrane only add to the overall complexity of this system and provide a real challenge to the validity of the model and the assumptions involved. The agreement between the model and experiments is excellent, with a maximum deviation of 12% for the multivalent ions, showing the robustness of the model and characterization studies. As shown in Fig. 13, the membrane performs surprisingly well for softening, selectively separating only the multivalent ions while passing along the monovalent ions. As seen earlier, the rejection increases with flux until a limiting value is reached.

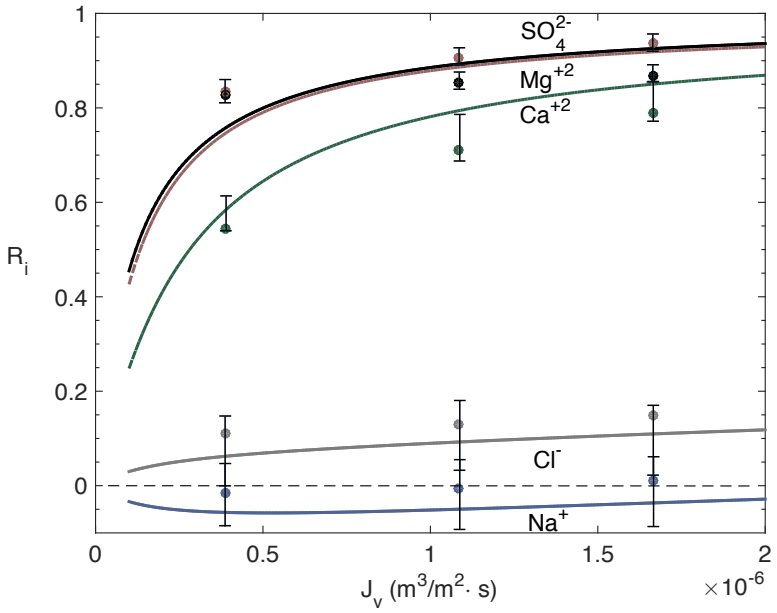

Figure 13: Experimental and modeling results for individual ion rejection in artificial seawater as a function of applied pressure and permeate flux. The maximum deviation between modeling and experimental results did not exceed 12% for multivalent ions, validating the model for this case. The error bars are based on 10% error in measuring the permeate concentration. Experimental values reported correspond to applied pressures of 2-4 bar. The high rejection of the LbL-C towards multivalent ions exclusively demonstrate its potential for implementation in desalination pretreatment. SO_4^{2-} is rejected more than Ca^{+2} in spite of its smaller Stokes radius/higher diffusivity by virtue of electrostatic interactions given the membrane's negative charger under these operating conditions.

Although to a lesser extent, negative rejection still occurs in this system and can be explained by an account similar to that of synthetic water mixtures. To simplify our analysis to first approximation, we consider the membrane is impermeable to all multivalent ions, which include Mg^{+2}, Ca^{+2}, and SO_4^{2-}. On the feed side, the concentration of Cl^- exceeds that of all other ions in the system. Faced by the membrane's relatively low retention, Cl^- is transported from feed to permeate down its gradient in electrochemical potential. Na^+ is the only ion available to keep the permeate solution electroneutral; and as a result, an excess of Na^+ ions appears in the permeate relative to the feed, leading to negative rejection.

While this account explains rejection, and why Na^+ is rejected less than Cl^-, it falls short of explaining why the multivalent ions are rejected in this particular order. Focusing on the two multivalent cations,

Mg^{+2} is rejected more than Ca^{+2} by virtue of its larger Stokes radius and lower diffusivity as shown in Table 2. Membrane charge becomes important when explaining why SO_4^{2-} is rejected at its current level. Being negatively charged under these feed conditions, the membrane rejects SO_4^{2-} more than Ca^{+2} by virtue of the resulting electrical interactions, in spite of sulfate's lower Stokes radius and higher diffusivity compared to calcium. An analysis similar to ours could help elucidate the trends observed in other publications for NF rejection on feeds featuring multi-ionic solutions, which becomes increasingly important for NF applications in softening and desalination [59, 60].

4.3. Investigating the Membrane Selectivity: Sensitivity Analysis

In addition to our previous analysis on the LbL-C membrane, the DSPM-DE model enables us to probe what characteristics dominate the separation performance, expands our understanding of NF membranes and their selective rejection towards multivalent ions, and explains why this membrane specifically is superior when it comes to low-pressure softening. Although the selectively high rejection of NF membranes towards multivalent ions is well-documented in literature, no formal attempt has been made, to the best of our knowledge, to ascertain what mechanism or which membrane property is responsible for this very unique selectivity. In this section, we propose an approach based on sensitivity analysis to answer this question.

By taking any mixture from Table 6 as our model solution and running sensitivity analysis varying the membrane characteristics from their nominal values reported in Table 5 and Section 4.1.4, the characteristics that dictate the separation performance can be identified. The main assumption underlying this analysis is the independence of the membrane characteristics from one another, which is reasonable given the scope of this sensitivity analysis.

Figure 14 illustrates the results obtained from running such an analysis, assuming NaCl+$MgCl_2$ is the model solution and taking increments of 20% from the nominal values of each membrane parameter. These results suggest that the membrane softening performance is not a strong function of the effective thickness, or more surprisingly, membrane charge density in this case. In contrast, varying the membrane effective pore size or pore dielectric constant can have a dramatic impact on softening performance, or multivalent ion retention, with greater dependence on the pore dielectric constant. Decreasing the membrane pore size makes the membrane relatively tighter, leading to higher rejections for any given flux. The increase in rejection, however, comes at an expense as the flux for any given pressure is expected to decline with a tighter membrane. Likewise, decreasing the pore dielectric constant also increases rejection as the ions experience a greater barrier to solvation, in accordance with the Born model.

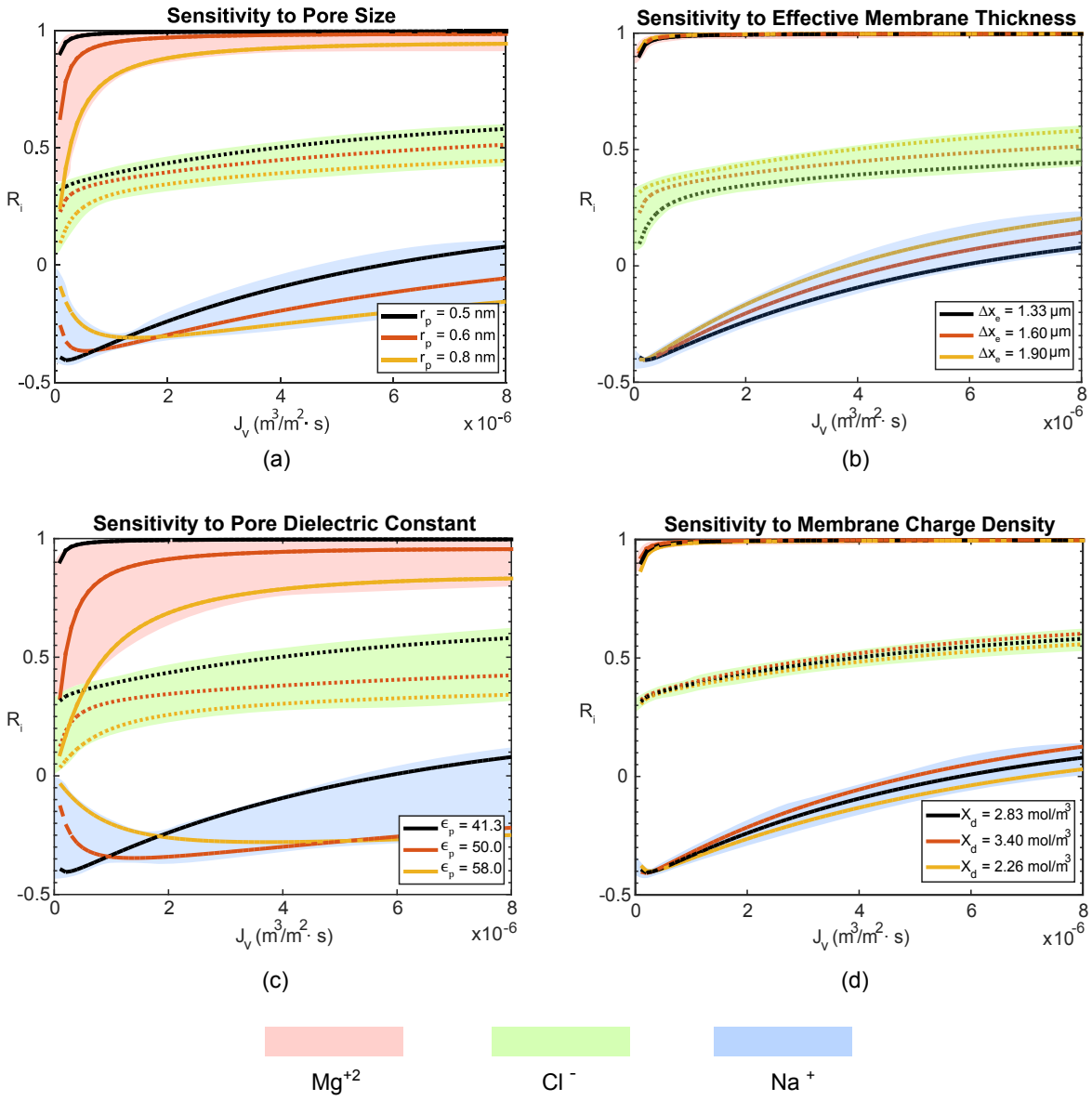

Figure 14: Results of the sensitivity analysis applied to the LbL-C membrane by varying: (a) the effective pore size; (b) the effective thickness; (c) the pore dielectric constant; and (d) the membrane charge density. The NaCl+$MgCl_2$ salt mixture was chosen as the model solution, and 20% increments from the nominal membrane parameters were taken. The results indicate the membrane softening performance and high selectivity towards monovalent ions is dominated by the pore dielectric constant, followed by the effective pore size, charge density, and finally the thickness.

Similar trends have been observed when this analysis was extended to the other mixtures in the study. In all cases, the membrane pore dielectric constant played the biggest role, followed by the effective pore size, charge density, and finally the membrane thickness. These findings underscore the importance of dielectric exclusion and steric hindrance as partitioning mechanisms in softening applications, and indicate that it is the right combination of these properties that are mostly responsible for the observed softening performance.

The conclusion that the selectively high rejection of NF membranes for multivalent ions is not dominated by membrane charge, but by the pore dielectric constant and pore size, is backed by empirical evidence in our study. For all synthetic water feeds considered, including artificial seawater, which had multivalent cations and anions, the multivalent ion retention was consistently higher relative to monovalent ions across all cases. Our methodology could potentially be extended to other NF membranes, and help provide a better understanding of the physics behind the NF separation process.

5. Conclusions

In this work, the Donnan-Steric Pore Model with dielectric exclusion (DSPM-DE) was applied for the first time to model the performance of a novel NF membrane, fabricated in-house using layer-by-layer (LbL) deposition with chemical crosslinking. The objective of this study has been to extend our understanding of low-pressure NF as it applies to water softening, and to elucidate what makes the LbL-C membrane particularly suited for this application. To accurately model the membrane performance, several experiments were conducted on a wide spectrum of feed chemistries, ranging from uncharged solutes to single salts, salt mixtures, and artificial seawater.

The membrane has been characterized based on the DSPM-DE model, and modeling results were then validated with experimental results. The notable agreement between experimental and modeling results demonstrate the success of the model and the membrane characterization technique adopted. The modeling results were later used to explain the trends observed, and elucidate the nature of the multi-ionic interactions that underlie the membrane's selectivity, and in particular negative rejection. An approach based on sensitivity analysis was finally introduced to ascertain which membrane parameter dominates the high selectivity of NF membranes for monovalent ions, and dictate the superior softening capacity of the LbL-C membrane. The key findings of our study can be summarized as follows:

1. Solute retention increases with increasing permeate flux, until a limiting rejection value, characteristic of the solute and the membrane, is reached. Beyond this point, any increase in the solvent convective transport is offset by the increasing solute transport. Solutes with greater retentions approached their limiting rejections at faster rates.
2. Uncharged solute rejection increased with increasing solute size, decreasing diffusivity, and increasing molecular weight, indicating that sieving effects dominated the separation process. A plot of uncharged solute rejection as a function of molecular weight can be used to estimate the MWCO of a NF membrane based on simulation results.
3. Negative rejection of the more mobile ion in a mixture, as observed in our softening experiments, is a result of kinetic effects, and stems from the fundamental requirements of charge electroneutrality and zero electric current traveling through the membrane.
4. For artificial seawater, the sequence of multivalent ion rejection of the LbL-C was Mg^{+2}, SO_4^{2-}, Ca^{+2}, which is a result of the interplay between the ion's Stokes radius, diffusivity, and membrane charge.

5. Low-pressure NF softening is only possible as a result of a membrane's ability to selectively "pick" the multivalent ions out of the solution, while allowing monovalent ions to pass through by design. This characteristic eliminates the additional energy penalties incurred by the unnecessary separation of monovalent in addition to multivalent ions in softening.
6. Zero or negative rejection of monovalent ions could prove advantageous in softening applications by increasing the osmotic pressure on the permeate side, leading to lower driving force requirements for a given permeate flux.
7. The selectively high rejection of NF membranes towards multivalent ions is largely dominated by the pore dielectric constant. For the LbL-C, selectivity was dominated by the pore dielectric constant, followed by the pore size, charge density, and lastly membrane thickness.

Acknowledgements

This research is supported by the National Research Foundation (NRF) Singapore under its Campus for Research Excellence and Technological Enterprise (CREATE) programme. The Center for Environmental Sensing and Modeling (CENSAM) is an interdisciplinary research group (IRG) of the Singapore MIT Alliance for Research and Technology (SMART) centre. The authors acknowledge Yagnaseni Roy for the technical support received on NF modeling, and Karim M. Chehayeb and Emily W. Tow for sharing their insights on multi-ionic solute interactions and negative rejection. Omar Labban also acknowledges the funding received by an MIT Pappalardo fellowship.

References

[1] P. Eriksson, Nanofiltration extends the range of membrane filtration, Environmental Progress 7 (1) (1988) 58–62. doi:10.1002/ep.3300070116.
URL http://dx.doi.org/10.1002/ep.3300070116

[2] M. Sen, A. Manna, P. Pal, Removal of arsenic from contaminated groundwater by membrane-integrated hybrid treatment system, Journal of Membrane Science 354 (1–2) (2010) 108 – 113. doi:10.1016/j.memsci.2010.02.063.
URL http://www.sciencedirect.com/science/article/pii/S0376738810001857

[3] I. Musbah, D. Cicéron, A. Saboni, S. Alexandrova, Retention of pesticides and metabolites by nanofiltration by effects of size and dipole moment, Desalination 313 (2013) 51 – 56. doi:10.1016/j.desal.2012.11.016.
URL http://www.sciencedirect.com/science/article/pii/S001191641200611X

[4] S. Phuntsho, S. Hong, M. Elimelech, H. K. Shon, Forward osmosis desalination of brackish groundwater: Meeting water quality requirements for fertigation by integrating nanofiltration, Journal of Membrane Science 436 (2013) 1 – 15. doi:10.1016/j.memsci.2013.02.022.
URL http://www.sciencedirect.com/science/article/pii/S0376738813001415

[5] J. Luo, L. Ding, Y. Wan, P. Paullier, M. Y. Jaffrin, Application of nf-rdm (nanofiltration rotating disk membrane) module under extreme hydraulic conditions for the treatment of dairy wastewater, Chemical Engineering Journal 163 (3) (2010) 307 – 316. doi:10.1016/j.cej.2010.08.007.
URL http://www.sciencedirect.com/science/article/pii/S1385894710006959

[6] M. Liu, Z. Lü, Z. Chen, S. Yu, C. Gao, Comparison of reverse osmosis and nanofiltration membranes in the treatment of biologically treated textile effluent for water reuse, Desalination 281 (2011) 372 – 378. doi:10.1016/j.desal.2011.08.023.
URL http://www.sciencedirect.com/science/article/pii/S0011916411007247

[7] L. Andrade, F. Mendes, J. Espindola, M. Amaral, Nanofiltration as tertiary treatment for the reuse of dairy wastewater treated by membrane bioreactor, Separation and Purification Technology 126 (2014) 21 – 29. doi:10.1016/j.seppur.2014.01.056.
URL http://www.sciencedirect.com/science/article/pii/S1383586614000902

[8] L. D. Nghiem, A. I. Schäfer, M. Elimelech, Nanofiltration of hormone mimicking trace organic contaminants, Separation Science and Technology 40 (13) (2005) 2633–2649. arXiv:http://www.tandfonline.com/doi/pdf/10.1080/01496390500283340, doi:10.1080/01496390500283340.
URL http://www.tandfonline.com/doi/abs/10.1080/01496390500283340

[9] L. D. Nghiem, A. I. Schäfer, M. Elimelech, Pharmaceutical retention mechanisms by nanofiltration membranes, Environmental Science & Technology 39 (19) (2005) 7698–7705, pMID: 16245847. arXiv:http://dx.doi.org/10.1021/es0507665, doi:10.1021/es0507665.
URL http://dx.doi.org/10.1021/es0507665

[10] B. D. Stanford, H. S. Weinberg, Evaluation of on-site wastewater treatment technology to remove estrogens, nonylphenols, and estrogenic activity from wastewater, Environmental Science & Technology 44 (8) (2010) 2994–3001, pMID: 20345150. arXiv:http://dx.doi.org/10.1021/es903422b, doi:10.1021/es903422b.
URL http://dx.doi.org/10.1021/es903422b

[11] A. Mohammad, Y. Teow, W. Ang, Y. Chung, D. Oatley-Radcliffe, N. Hilal, Nanofiltration membranes review: Recent advances and future prospects, Desalination 356 (2015) 226 – 254, State-of-the-Art Reviews in Desalination. doi:10.1016/j.desal.2014.10.043.
URL http://www.sciencedirect.com/science/article/pii/S0011916414005773

[12] W. Fang, L. Shi, R. Wang, Interfacially polymerized composite nanofiltration hollow fiber membranes for low-pressure water softening, Journal of Membrane Science 430 (2013) 129 – 139. doi:10.1016/j.memsci.2012.12.011.
URL http://www.sciencedirect.com/science/article/pii/S0376738812009210

[13] W. Fang, L. Shi, R. Wang, Mixed polyamide-based composite nanofiltration hollow fiber membranes with improved low-pressure water softening capability, Journal of Membrane Science 468 (2014) 52 – 61. doi:10.1016/j.memsci.2014.05.047.
URL http://www.sciencedirect.com/science/article/pii/S0376738814004232

[14] H. Deng, Y. Xu, Q. Chen, X. Wei, B. Zhu, High flux positively charged nanofiltration membranes prepared by uv-initiated graft polymerization of methacrylatoethyl trimethyl ammonium chloride (dmc) onto polysulfone membranes, Journal of Membrane Science 366 (1–2) (2011) 363 – 372. doi:10.1016/j.memsci.2010.10.029.
URL http://www.sciencedirect.com/science/article/pii/S0376738810007982

[15] H. Zhang, H. Mao, J. Wang, R. Ding, Z. Du, J. Liu, S. Cao, Mineralization-inspired preparation of composite membranes with polyethyleneimine–nanoparticle hybrid active layer for solvent resistant nanofiltration, Journal of Membrane Science 470 (2014) 70 – 79. doi:10.1016/j.memsci.2014.07.019.
URL http://www.sciencedirect.com/science/article/pii/S037673881400547X

[16] C. Liu, L. Shi, R. Wang, Enhanced hollow fiber membrane performance via semi-dynamic layer-by-layer polyelectrolyte inner surface deposition for nanofiltration and forward osmosis applications, Reactive and Functional Polymers 86 (2015) 154 – 160. doi:10.1016/j.reactfunctpolym.2014.07.018.
URL http://www.sciencedirect.com/science/article/pii/S138151481400145X

[17] C. Liu, L. Shi, R. Wang, Crosslinked layer-by-layer polyelectrolyte nanofiltration hollow fiber membrane for low-pressure water softening with the presence of SO_4^{2-} in feed water, Journal of Membrane Science 486 (2015) 169 – 176. doi:10.1016/j.memsci.2015.03.050.
URL http://www.sciencedirect.com/science/article/pii/S0376738815002380

[18] V. Silva, V. Geraldes, A. B. Alves, L. Palacio, P. Prádanos, A. Hernández, Multi-ionic nanofiltration of highly concentrated salt mixtures in the seawater range, Desalination 277 (1–3) (2011) 29 – 39. doi:10.1016/j.desal.2011.03.088.
URL http://www.sciencedirect.com/science/article/pii/S0011916411003195

[19] M. Soltanieh, M. Mousavi, Application of charged membranes in water softening: modeling and experiments in the presence of polyelectrolytes, Journal of Membrane Science 154 (1) (1999) 53 – 60. doi:10.1016/S0376-7388(98)00285-3.
URL http://www.sciencedirect.com/science/article/pii/S0376738898002853

[20] M. Bodzek, S. Koter, K. Wesołowska, Application of membrane techniques in a water softening process, Desalination 145 (1–3) (2002) 321 – 327. doi:10.1016/S0011-9164(02)00430-7.
URL http://www.sciencedirect.com/science/article/pii/S0011916402004307

[21] K. Wesolowska, S. Koter, M. Bodzek, Modelling of nanofiltration in softening water, Desalination 162 (2004) 137 – 151. doi:10.1016/S0011-9164(04)00037-2.
URL http://www.sciencedirect.com/science/article/pii/S0011916404000372

[22] B. Saliha, F. Patrick, S. Anthony, Investigating nanofiltration of multi-ionic solutions using the steric, electric and dielectric exclusion model, Chemical Engineering Science 64 (17) (2009) 3789 – 3798. doi:10.1016/j.ces.2009.05.020.
URL http://www.sciencedirect.com/science/article/pii/S0009250909003431

[23] T. Tsuru, S. Nakao, S. Kimura, Calculation of ion rejection by extended Nernst–Planck equation with charged reverse osmosis membranes for single and mixed electrolyte solutions, Journal of Chemical Engineering of Japan 24 (4) (1991) 511–517. doi:10.1252/jcej.24.511.

[24] X.-L. Wang, T. Tsuru, S. Nakao, S. Kimura, Electrolyte transport through nanofiltration membranes by the space-charge model and the comparison with teorell-meyer-sievers model, Journal of Membrane Science 103 (1–2) (1995) 117 – 133. doi:10.1016/0376-7388(94)00317-R.
URL http://www.sciencedirect.com/science/article/pii/037673889400317R

[25] W. Bowen, H. Mukhtar, Characterisation and prediction of separation performance of nanofiltration membranes, Journal of Membrane Science 112 (2) (1996) 263 – 274. doi:10.1016/0376-7388(95)00302-9.
URL http://www.sciencedirect.com/science/article/pii/0376738895003029

[26] W. Bowen, A. Mohammad, N. Hilal, Characterisation of nanofiltration membranes for predictive purposes — use of salts, uncharged solutes and atomic force microscopy, Journal of Membrane Science 126 (1) (1997) 91 – 105. doi:10.1016/S0376-7388(96)00276-1.
URL http://www.sciencedirect.com/science/article/pii/S0376738896002761

[27] W. Bowen, A. Wahab Mohammad, Diafiltration by nanofiltration: Prediction and optimization, AIChE Journal 44 (8) (1998) 1799–1812. doi:10.1002/aic.690440811.
URL http://dx.doi.org/10.1002/aic.690440811

[28] J. Schaep, C. Vandecasteele, A. W. Mohammad, W. R. Bowen, Analysis of the salt retention of nanofiltration membranes using the donnan–steric partitioning pore model, Separation Science and Technology 34 (15) (1999) 3009–3030. arXiv:http://dx.doi.org/10.1081/SS-100100819, doi:10.1081/SS-100100819.
URL http://dx.doi.org/10.1081/SS-100100819

[29] W. Bowen, J. S. Welfoot, Modelling the performance of membrane nanofiltration—critical assessment and model development, Chemical Engineering Science 57 (7) (2002) 1121 – 1137. doi:10.1016/S0009-2509(01)00413-4.
URL http://www.sciencedirect.com/science/article/pii/S0009250901004134

[30] S. Bandini, D. Vezzani, Nanofiltration modeling: the role of dielectric exclusion in membrane characterization, Chemical Engineering Science 58 (15) (2003) 3303 – 3326. doi:10.1016/S0009-2509(03)00212-4.
URL http://www.sciencedirect.com/science/article/pii/S0009250903002124

[31] V. Geraldes, A. M. B. Alves, Computer program for simulation of mass transport in nanofiltration membranes, Journal of Membrane Science 321 (2) (2008) 172 – 182. doi:10.1016/j.memsci.2008.04.054.
URL http://www.sciencedirect.com/science/article/pii/S037673880800392X

[32] Y. Roy, M. H. Sharqawy, J. H. Lienhard V, Modeling of flat-sheet and spiral-wound nanofiltration configurations and its application in seawater nanofiltration, Journal of Membrane Science 493 (2015) 360 – 372. doi:10.1016/j.memsci.2015.06.030.
URL http://www.sciencedirect.com/science/article/pii/S0376738815300028

[33] R. W. Baker, Membrane Technology and Applications, John Wiley & Sons, Ltd, 2004. doi:10.1002/0470020393.
URL http://dx.doi.org/10.1002/0470020393

[34] W. M. Deen, Hindered transport of large molecules in liquid-filled pores, AIChE Journal 33 (9) (1987)

1409–1425. doi:10.1002/aic.690330902.
URL http://dx.doi.org/10.1002/aic.690330902

[35] P. Dechadilok, W. M. Deen, Hindrance factors for diffusion and convection in pores, Industrial & Engineering Chemistry Research 45 (21) (2006) 6953–6959. arXiv:http://dx.doi.org/10.1021/ie051387n, doi:10.1021/ie051387n.
URL http://dx.doi.org/10.1021/ie051387n

[36] G. M. Mavrovouniotis, H. Brenner, Hindered sedimentation, diffusion, and dispersion coefficients for brownian spheres in circular cylindrical pores, Journal of Colloid and Interface Science 124 (1) (1988) 269 – 283. doi:10.1016/0021-9797(88)90348-7.
URL http://www.sciencedirect.com/science/article/pii/0021979788903487

[37] J. Ennis, H. Zhang, G. Stevens, J. Perera, P. Scales, S. Carnie, Mobility of protein through a porous membrane, Journal of Membrane Science 119 (1) (1996) 47 – 58. doi:10.1016/0376-7388(96)00112-3.
URL http://www.sciencedirect.com/science/article/pii/0376738896001123

[38] L. R. Glicksman, J. H. Lienhard V, Modeling and Approximation in Heat Transfer, Cambridge University Press, 2016.
URL http://www.cambridge.org/9781107012172

[39] S. Sablani, M. Goosen, R. Al-Belushi, M. Wilf, Concentration polarization in ultrafiltration and reverse osmosis: a critical review, Desalination 141 (3) (2001) 269 – 289. doi:10.1016/S0011-9164(01)85005-0.
URL http://www.sciencedirect.com/science/article/pii/S0011916401850050

[40] V. Geraldes, M. D. Afonso, Prediction of the concentration polarization in the nanofiltration/reverse osmosis of dilute multi-ionic solutions, Journal of Membrane Science 300 (1–2) (2007) 20 – 27. doi:10.1016/j.memsci.2007.04.025.
URL http://www.sciencedirect.com/science/article/pii/S0376738807002815

[41] A. I. Schäfer, A. G. Fane, T. D. Waite, Nanofiltration: principles and applications, Elsevier, 2005.

[42] A. Grodzinsky, Field, Forces and Flows in Biological Systems, Garland Science, 2011.

[43] F. G. Donnan, Theory of membrane equilibria and membrane potentials in the presence of non-dialysing electrolytes. a contribution to physical-chemical physiology, Journal of Membrane Science 100 (1) (1995) 45–55.

[44] K. Dill, S. Bromberg, Molecular driving forces: statistical thermodynamics in biology, chemistry, physics, and nanoscience, Garland Science, 2010.

[45] D. L. Parkhurst, C. Appelo, User's guide to PHREEQC (Version 2): A computer program for speciation, batch-reaction, one-dimensional transport, and inverse geochemical calculations.

[46] K. H. Mistry, H. A. Hunter, J. H. Lienhard V, Effect of composition and nonideal solution behavior on desalination calculations for mixed electrolyte solutions with comparison to seawater, Desalination 318 (2013) 34 – 47. doi:10.1016/j.desal.2013.03.015.
URL http://www.sciencedirect.com/science/article/pii/S0011916413001409

[47] R. Silbey, R. Alberty, M. Bawendi, Physical Chemistry 4th edn, Wiley, New York, 2004.

[48] J. C. Giddings, E. Kucera, C. P. Russell, M. N. Myers, Statistical theory for the equilibrium distribution of rigid molecules in inert porous networks. exclusion chromatography, The Journal of Physical Chemistry 72 (13) (1968) 4397–4408. arXiv:http://dx.doi.org/10.1021/j100859a008, doi:10.1021/j100859a008.
URL http://dx.doi.org/10.1021/j100859a008

[49] A. E. Yaroshchuk, Dielectric exclusion of ions from membranes, Advances in Colloid and Interface Science 85 (2–3) (2000) 193 – 230. doi:10.1016/S0001-8686(99)00021-4.
URL http://www.sciencedirect.com/science/article/pii/S0001868699000214

[50] L. Shi, S. Chou, R. Wang, W. Fang, C. Tang, A. Fane, Effect of substrate structure on the performance of thin-film composite forward osmosis hollow fiber membranes, Journal of Membrane Science 382 (1–2) (2011) 116 – 123. doi:10.1016/j.memsci.2011.07.045.
URL http://www.sciencedirect.com/science/article/pii/S0376738811005710

[51] C. Liu, W. Fang, S. Chou, L. Shi, A. G. Fane, R. Wang, Fabrication of layer-by-layer assembled FO hollow fiber membranes and their performances using low concentration draw solutions, Desalination 308 (2013) 147 – 153, new Directions in Desalination. doi:10.1016/j.desal.2012.07.027.
URL http://www.sciencedirect.com/science/article/pii/S0011916412003980

[52] W. Bowen, A. Mohammad, Characterization and prediction of nanofiltration membrane performance—a general assessment, Chemical Engineering Research and Design 76 (8) (1998) 885 – 893, separation Processes. doi:10.1205/026387698525685.
URL http://www.sciencedirect.com/science/article/pii/S0263876298717253

[53] N. S. Kotrappanavar, A. Hussain, M. Abashar, I. S. Al-Mutaz, T. M. Aminabhavi, M. N. Nadagouda, Prediction of physical properties of nanofiltration membranes for neutral and charged solutes, Desalination 280 (1–3) (2011) 174 – 182. doi:10.1016/j.desal.2011.07.007.
URL http://www.sciencedirect.com/science/article/pii/S0011916411006217

[54] R. Rautenbach, A. Gröschl, Separation potential of nanofiltration membranes, Desalination 77 (1990) 73–84.

[55] J. Garcia-Aleman, J. M. Dickson, Permeation of mixed-salt solutions with commercial and pore-filled nanofiltration membranes: membrane charge inversion phenomena, Journal of Membrane Science 239 (2) (2004) 163 – 172. doi:10.1016/j.memsci.2004.02.036.
URL http://www.sciencedirect.com/science/article/pii/S037673880400184X

[56] T. Tsuru, M. Urairi, S.-I. Nakao, S. Kimura, Negative rejection of anions in the loose reverse osmosis separation of mono-and divalent ion mixtures, Desalination 81 (1-3) (1991) 219–227.

[57] W. R. Bowen, J. S. Welfoot, P. M. Williams, Linearized transport model for nanofiltration: Development and assessment, AIChE Journal 48 (4) (2002) 760–773. doi:10.1002/aic.690480411.
URL http://dx.doi.org/10.1002/aic.690480411

[58] A. E. Yaroshchuk, Negative rejection of ions in pressure-driven membrane processes, Advances in Colloid and Interface Science 139 (1–2) (2008) 150 – 173, membrane Electrochemistry: Selected papers from the 33rd Conference on Membrane Electrochemistry, Russia, May 2007. doi:10.1016/j.cis.2008.01.004.
URL http://www.sciencedirect.com/science/article/pii/S0001868608000328

[59] M. Park, J. Park, E. Lee, J. Khim, J. Cho, Application of nanofiltration pretreatment to remove divalent ions for economical seawater reverse osmosis desalination, Desalination and Water Treatment (2015) 1–10arXiv:http://dx.doi.org/10.1080/19443994.2015.1111807, doi:10.1080/19443994.2015.1111807.
URL http://dx.doi.org/10.1080/19443994.2015.1111807

[60] A. M. Mika, R. F. Childs, J. M. Dickson, Ultra-low pressure water softening: a new approach to membrane construction, Desalination 121 (2) (1999) 149 – 158. doi:10.1016/S0011-9164(99)00016-8.
URL http://www.sciencedirect.com/science/article/pii/S0011916499000168